Article

Brown Adipose Tissue and Skeletal Muscle Coordinately Contribute to Thermogenesis in Mice

Yuna Izumi-Mishima,[1] Rie Tsutsumi,[1] Tetsuya Shiuchi,[2] Saori Fujimoto,[1] Momoka Taniguchi,[1] Mizuki Sugiuchi, [1] Manaka Tsutsumi, [1] Yuko Okamatsu-Ogura,[3] Takeshi Yoneshiro,[4] Masashi Kuroda,[1] Kazuhiro Nomura,[1] and Hiroshi Sakaue[1,5,*]

[1]Department of Nutrition and Metabolism, Institute of Biomedical Sciences, Tokushima University Graduate School, Tokushima 770-8503, Japan
[2]Department of Integrative Physiology, Institute of Biomedical Sciences, Tokushima University Graduate School, Tokushima 770-8503, Japan
[3]Laboratory of Biochemistry, Faculty of Veterinary Medicine, Hokkaido University, Sapporo 060-0818, Japan
[4]Division of Molecular Physiology and Metabolism, Tohoku University Graduate School of Medicine, Sendai 980-8575, Japan
[5]Lead contact
*Correspondence: hsakaue@tokushima-u.ac.jp

Abstract

Endotherms increase the rate of metabolism in metabolic organs as one strategy to cope with a decline in temperature of the external environment. However, an additional major contributor to maintenance of body temperature in a cold environment is contraction-based thermogenesis in skeletal muscle. Here, we show that impairment of hind limb muscle contraction by cast immobilization induced a loss of function of skeletal muscle and activated brown adipose tissue (BAT) thermogenesis as a compensatory mechanism. BAT utilizes free branched-chain amino acids (BCAAs) derived from skeletal muscle as an energy substrate for thermogenesis, and interleukin-6 released by skeletal muscle stimulates BCAAs production in muscle for support of BAT thermogenesis. Additionally, this thermoregulatory system between BAT and skeletal muscle may also play an important role in response to cold temperatures or acute stress. Our findings suggest that BAT and skeletal muscle cooperate to maintain body temperature in endotherms.

Introduction

Endotherms rely on the regulation of heat generation by metabolism in tissues of the body to maintain a stable core body temperature in the face of a fluctuating temperature of the external environment and thereby to ensure optimal physiological function.[1] Small mammals adjust their metabolic rate to cope with temperature fluctuations and to support their survival during seasonal acclimation. Some mammalian species are able to lower their metabolic rate and enter a state of torpor or hibernation in order to conserve energy and ensure survival.[2] However, small mammals that do not hibernate must increase their rate of metabolism, including obligatory thermogenesis in metabolic organs such as the liver and skeletal muscle as well as regulatory thermogenesis (shivering or nonshivering thermogenesis) in skeletal muscle and brown adipose tissue (BAT), in order to maintain thermal homeostasis in a cold environment.[1,3,4]

Under normothermic conditions, core body temperature is determined by basal metabolic organs such as the brain, heart, liver, and skeletal muscle. [1] Skeletal muscle is the largest weight-bearing organ in humans and consumes a substantial amount of energy, even at rest. Shivering is the major source of heat production in acute cold exposure before sufficient amount of UCP1 (uncoupling protein 1) can be recruited in BAT[1,5,6]. Shivering is gradually replaced by UCP1 dependent thermogenesis and nonshivering thermogenesis is necessary for long-term adaptation to a cold environment. [5] Skeletal muscle and BAT thermogenesis can compensate in part each other to maintain core body temperature is widely recognaized[5-8], and recent study suggests that suppression of BAT thermogenesis has been found to promote thermogenesis in skeletal muscle.[8]

While skeletal muscle is the critical metabolic organ, it also stores an abundance of amino acids as energy substrates in the form of muscle proteins.[9] Skeletal muscle also has the plasticity for adapting to environmental conditions and shows metabolic flexibility in response to the substrate requirements of other organs and thereby contributes to the maintenance of energy balance.[9,10] Activation of BAT themogenesis is associated with increased lipid and glucose catabolism.[11-13] Succinate and branched-chain amino acids (BCAAs) have also been found to support BAT thermogenesis, however.[14–16] Although succinate may be provided by muscle contraction,[14,17] the primary source of BCAAs for BAT thermogenesis has remained unclear. Indeed, mitochondrial BCAAs

catabolism in brown adipocytes promotes systemic BCAAs clearance. Skeletal muscle may therefore also respond to the energy demands of BAT.

Whereas body temperature and energy metabolism in metabolic organs are closely related, how they are regulated in a coordinated manner is poorly understood. Several endocrine factors alter metabolism in abdominal organs.[18] In particular, interleukin (IL)–6 is an endocrine factor that plays multiple roles in the response of the body to infection, exercise, and stress as well as in inflammation.[19–21] IL-6 induces various fever responses, including nonshivering thermogenesis in BAT, by promoting prostaglandin E2 (PGE2) synthesis in central vascular endothelial cells.[22] On the other hand, IL-6 directly affects energy metabolism in various organs, including skeletal muscle, liver, and adipose tissue.[23–27] These multiple roles suggest that IL-6 is a key molecule linking thermogenesis and energy metabolism.

Here we show that a loss of skeletal muscle function by cast immobilization in mice activates a compensatory thermoregulatory system dependent on BAT thermogenesis. We also show that free BCAAs derived from skeletal muscle support BAT thermogenesis, and we identify IL-6 as a key regulator of this system. Our findings reveal the importance of skeletal muscle as a source of amino acids and uncover a previously unrecognized thermoregulatory system mediated by BAT and skeletal muscle metabolism.

Results

Cast immobilization activates a compensatory thermoregulatory system

We first examined the role of skeletal muscle in endothermic homeostasis by performing an acute cold tolerance test at 4°C for 4 h in mice with both hind limbs immobilized in casts. We confirmed that ~50% of systemic skeletal muscle was immobilized (Table S1), and that the immobilization induced skeletal muscle atrophy within 3 to 5 days (Figure 1_figure supplement 1A–1C). Systemic locomotor activity was decreased during dark phase in cast immobilized mice compared to control mice (Figure1_ figure supplement 1D and 1E). Hence, the core body temperature showed a tended to decrease in cast-immobilized mice compared to control mice under room temperature (Figure 1_figure supplement 1F). Mice with both hind limbs immobilized for 7 days showed a significantly lower core body temperature after cold exposure compared with control mice (Figure 1A). Cast immobilization for 24 h also induced cold intolerance with preservation of muscle mass (Figure 1B and

Figure 1_figure supplement 1A-1C). Expression of *Ucp1* mRNA in interscapular BAT (iBAT) was significantly increased after cold exposure in control mice, whereas those expression were not induced by cold exposure in cast immobilized mice (Figure 1_figure supplement 1G). Although the amount of *Sln* (sarcolipin) mRNA in immobilized muscle was not increased by acute cold exposure, expression of *Ucp2*, *Ucp3* and *Ppargc1a* (PGC-1α) were significantly increased in control mice but not in cast-immobilized mice (Figure 1_fugure supplement 1H-1K). To investigate whether cold intolerance depends on the immobilized muscle mass, we examined the change in core body temperature in mice with unilateral immobilization. Systemic locomotor activity during cold exposure was similar for mice with unilateral or bilateral immobilization and for control mice (Figure 1_figure supplement 1L). However, the decrease in body temperature induced by cold exposure in mice with unilateral immobilization was attenuated compared with that in mice subjected to bilateral immobilization (Figure 1C). These findings suggested that immobilization of skeletal muscle suppresses thermogenesis in this organ independently of systemic locomotor activity.

To investigate the mechanism underlying the maintenance of core body temperature in mice with cast immobilization, we examined the effects of such immobilization on skeletal muscle and BAT. Metabolomic profiling of the immobilized muscle revealed decreases in the amounts of fumaric acid and malic acid within 1 day of cast immobilization (Figure 1_fugure supplement 2A). The amount of *Ucp3* mRNA increased transiently in immobilized muscle before returning to baseline levels, whereas that of *Ucp2* mRNA was not affected until 5 days of cast immobilization (Figure 1_figure supplement 2B and 2C). Sarcolipin signaling has been shown to promote mitochondrial biogenesis and oxidative metabolism via activation of Ca^{2+}- and calmodulin-dependent protein kinase II (CaMKII) and PGC-1α in skeletal muscle.[28] However, we found that expression of the *Sln, Camk2a*, *Ppargc1a* (PGC-1α), and *Tfam* (transcription factor A, mitochondrial) genes was not increased in immobilized muscle (Figure 1_figure supplement 2D-2G). These findings thus suggested that nonshivering thermogenesis was induced minimally in cast-immobilized skeletal muscle. On the other hand, expression of UCP1 at the mRNA and protein levels as well as the abundance of PGC-1α, a transcriptional cofactor that promotes the expression of thermogenesis-related genes, showed transient increases in iBAT after cast immobilization (Figures 1E–1G). Small and multilocular lipid droplets were apparent in adipocytes of iBAT within 24 h of cast immobilization (Figure

1_figure supplement 2H). However, mice subjected to cast immobilization showed no increase in food consumption or systemic activity levels (Figure 1_figure supplement 1D and 1E and 2I). These results indicated that the suppression of muscle thermogenesis by cast immobilization induces BAT thermogenesis without an increase in food consumption or systemic activity levels. Cast immobilization thus preferentially activated nonshivering thermogenesis in BAT, not in skeletal muscle.

Cast immobilization promotes BAT thermogenesis via sympathetic activation

We next explored the mechanism underlying the activation of BAT thermogenesis by cast immobilization. We first focused on the sympathetic nervous system, a general inducer of BAT thermogenesis,[29] and found that the norepinephrine concentration in iBAT was tended to increase transiently after 24 h of cast immobilization (Figure 1H). We then subjected mice to sympathetic denervation of iBAT. Expression of *Ucp1* mRNA in iBAT was significantly attenuated by such denervation in mice with or without subsequent cast immobilization (Figure 1I). Whereas adipocytes of iBAT showed small and multilocular lipid droplets after 7 days of cast immobilization in sham-operated mice, iBAT of mice subjected to surgical denervation was hypertrophied and did not show such lipid droplets (Figure 1_figure supplement 2J). Moreover, mice with denervated iBAT manifested a lower core body temperature compared with sham-operated mice after cold exposure at 4°C for 1 h, and cast immobilization further increased the extent of hypothermia in the denervated mice (Figure 1J). These results suggested that BAT thermogenesis is activated via sympathetic nerves to maintain core body temperature in cast-immobilized mice.

Cast immobilization alters systemic metabolic dynamics associated with BAT thermogenesis

We next examined the metabolic dynamics of iBAT as well as systemic metabolic changes in mice subjected to cast immobilization. Previous study suggests that acute cold exposure on mice increases the free amino acids concentration and carbohydrate metabolites such as the glycolysis pathway, the pentose phosphate pathway and the tricarboxylic acid (TCA) cycle in BAT.[30] Consistent with previous findings, metabolomics analysis revealed increases in the amounts of carbohydrate metabolites and amino acids in iBAT that were

apparent as early as 10 h after cast immobilization, and several glucose and amino acid metabolic pathways were significantly activated (Figure 2_figure supplement 1A).Increases in these metabolites after cast immobilization were not apparent in mice with iBAT denervation (Figures 2A and 2B). Brown adipocytes incorporate fatty acids and various other energy substrates to initiate thermogenesis and contribute to the maintenance of core body temperature.[31] We found that expression of the genes for fatty acid (Figure 2C) and succinate (Figure 2D) transporters in iBAT was induced by cast immobilization and that such induction was prevented by iBAT denervation. The concentration of succinate was also increased in iBAT of cast-immobilized mice in a manner sensitive to iBAT denervation (Figure 2E). Consistent with these changes in metabolite levels, oxygen consumption and systemic lipid utilization were increased by cast immobilization in intact mice (Figures 2F and 2G) but not in those subjected to iBAT denervation (Figure 2_figure supplement 1B and 1C).

The weight of epididymal white adipose tissue (eWAT) and hepatic glycogen content were reduced by cast immobilization (Figures 2H and 2I). Expression of the genes for glucose-6-phosphatase (G6Pase) and phosphoenolpyruvate carboxykinase (PEPCK) in the liver increased gradually after cast immobilization, peaking at day 5 (Figure 2_figure supplement 2A and 2B), suggesting that gluconeogenesis was slowly activated in the cast-immobilized mice. Metabolomic profiling of the liver revealed marked increases in the amounts of 3-phosphoglyceric acid and 2-phosphoglyceric acid within 1 day of cast immobilization (Figure 2_figure supplement 2C), suggesting that glycerol influx was also enhanced in the liver. Together, these results thus indicated that cast immobilization affects metabolic dynamics in the liver and WAT, and that these changes might occur after the activation of BAT thermogenesis.

The serum concentration of noradrenaline was increased within 1 day of cast immobilization (Figure 2_figure supplement 2D), but these metabolic changes induced by cast immobilization were not associated with by an increase in the serum concentration of corticosterone or in expression of the gene for corticotropin-releasing hormone (CRH) in the hypothalamus (Figure 2_figure supplement 1E and 1F). These results suggest that cast immobilization may activates BAT thermogenesis and systemic metabolic changes through lower body temperature resulting from suppression of muscle thermogenesis rather than stress.

Free amino acids are transferred from skeletal muscle to BAT and the liver for energy homeostasis

We next focused on metabolism of amino acids in BAT and skeletal muscle in mice after cast immobilization. As shown above, amino acid concentrations in iBAT were increased by cast immobilization in a manner sensitive to denervation of iBAT (Figure 2B and Figure 2_figure supplement 1A). The amounts of free amino acids were also increased in both soleus and extensor digitorum longus (EDL) muscles of cast-immobilized mice (Figure 3A), whereas those in serum and the liver were not increased by cast immobilization (Figure 3B). Consistent with previous findings,[32] we found that gene expression for the ubiquitin ligases Atrogin-1 and MuRF-1 was increased during the early phase (days 1–3) of cast immobilization (Figure 3_figure supplement 1A and 1B). We then examined gene expression profiles for solute carrier (SLC) transporters that mediate the transport of amino acids across cell membranes as well as for mitochondrial BCAA catabolic enzymes (BCAT2, branched-chain aminotransferase 2; BCKDHA, branched-chain keto acid dehydrogenase E1 subunit α) in iBAT, liver, and soleus. Expression of the genes for SLC1A5 (a sodium-dependent glutamate transporter) and SLC38A2 (a sodium-coupled neutral amino acid transporter) was significantly increased in iBAT after cast immobilization for 10 h (Figure 3_figure supplement 1C–1H). In the liver, expression of the gene for SLC38A2, which is upregulated by extracellular amino acid deprivation,[33,34] and of that for BCKDHA, which is thought to be upregulated under fasting conditions to oxidize BCAAs for gluconeogenesis,[35,36] was significantly increased by cast immobilization (Figure 3_figure supplement 1I–1M). On the other hand, gene expression for amino acid transporters (SLC1A5, SLC7A5, SLC38A2) and BCAAs catabolic enzymes (BCAT2, BCKDHA) in soleus was significantly decreased after cast immobilization (Figure 3_figure supplement 1N–1S). Expression of the gene for SLC43A1, which is upregulated by food deprivation and is thought to transport amino acids from cells to the external environment,[37] was significantly increased in soleus by cast immobilization (Figure 3_figure supplement 1Q).

We next investigated amino acid incorporation in tissues by administration of [^{3}H]leucine into the tail vein of mice. Incorporation of [^{3}H]leucine was not increased in skeletal muscle of mice subjected to cast immobilization for 1 or 3 days (data not shown), whereas it was significantly increased in iBAT, liver, and kidney of those subjected to cast immobilization for

1 day (Figure 3C). Gene expression for SLC25A44, a mitochondrial BCAAs transporter that contributes to BAT thermogenesis,[15] was increased in iBAT at 24 h after cast immobilization (Figure 3D and Figure 3_figure supplement 2A-2C). However, the early increases in expression of the genes for SLC25A44, SLC1A5, and SLC38A2 induced by cast immobilization in iBAT of intact mice were prevented by denervation of iBAT (Figure 3D and Figure 3_figure supplement 1D–1J). Our results thus suggested that free amino acids are utilized as an energy substrate in BAT and the liver rather than in skeletal muscle of cast-immobilized mice.

Cast immobilization upregulates IL-6 gene expression in BAT and skeletal muscle

We next set out to identify regulatory molecules that might contribute to the maintenance of body temperature and to the systemic metabolic changes in cast-immobilized mice. Gene expression analysis revealed that the IL-6 gene tended to be induced earlier and to a greater extent in iBAT and soleus than were genes for other cytokines including tumor necrosis factor–α (TNF-α), monocyte chemoattractant protein–1 (MCP-1), IL-1β, IL-10, and IL-15; for batokines including fibroblast growth factor 21 (FGF21) and bone morphogenetic protein 8B (BMP8B); or for myokines including FGF21 and irisin (Figures 4A–4D and Figure 4_figure supplement 1A–1N). Whereas the increase in the amount of *Il6* mRNA was apparent as early as 6 to 10 h in iBAT, that in soleus was more gradual (Figures 4C and 4D). IL-6 has been found to be released by various organs, including adipose tissue and skeletal muscle, in response to inflammation, stress, or exercise.[18-21] The abundance of *Il6* mRNA in liver, eWAT, or spleen was not affected by cast immobilization (Figure 4_figure supplement 1O–1Q). Expression of the genes for serum amyloid A3 (*Saa3*) and suppressor of cytokine signaling 3 (*Socs3*), both of which are regulated by IL-6 signaling, was also increased in iBAT and soleus at the same time as was that of *Il6* (Figures 4E–4H). Expression of these genes was also increased in the liver or eWAT at 10 or 24 h after cast immobilization (Figures 4I–4L). However, expression of *Il6* was not induced by cast immobilization in denervated iBAT (Figures 4M). The serum concentration of IL-6 was significantly increased from 10 h after cast immobilization (Figure 4N), whereas that of TNF-α was not altered in cast-immobilized mice (Figure 4_figure supplement 1R). Together, these results suggested that cast immobilization induces *Il6* expression in iBAT and skeletal muscle, and that induction of *Il6*

expression by cast immobilization in iBAT is dependent on the sympathetic nervous system.

IL-6 affects energy metabolism in BAT and skeletal muscle of cast-immobilized mice

We investigated the role of IL-6 in the skeletal muscle–BAT thermoregulatory system with the use of subjected IL-6 knockout (KO) mice to cast immobilization. Expression of *Ucp1* in iBAT was significantly increased at 24 h after cast immobilization in both WT and IL-6 KO mice (Figure 5_figure supplement 1A). However, core body temperature of cast-immobilized IL-6 KO mice was decreased to a greater extent by cold exposure at 4°C for 4 h compared with that of cast-immobilized WT mice (Figure 5A). Furthermore, unlike that in WT mice, oxygen consumption was not increased in IL-6 KO mice after cast immobilization (Figure 5_figure supplement 1B and 1C). Metabolomics analysis revealed that the amounts of carbohydrate metabolites including glucose 1-phosphate, glucose 6-phosphate, and phosphoenolpyruvic acid in iBAT were higher for IL-6 KO mice than for WT mice and were not increased substantially by cast immobilization in the mutant mice (Figure 5B). Whereas the concentrations of amino acids such as Ser, Asn, Lys, Met, His, Phe, and Tyr in iBAT of WT mice were increased markedly at 24 h after cast immobilization, such was not the case for IL-6 KO mice (Figure 5C). Expression of the genes for SLC25A44, BCKDHA, and CD36 in iBAT was higher for IL-6 KO mice than for WT mice, but expression of the genes for SLC25A44 and CD36 in iBAT of IL-6 KO mice was not increased further at 24 h after cast immobilization (Figures 5D–5F). Incorporation of [^{3}H]leucine was also not increased in iBAT of IL-6 KO mice after cast immobilization for 24 h (Figure 5G). In addition, adipocytes with small and multilocular lipid droplets were observed in iBAT of IL-6 KO mice with or without cast immobilization (Figure 5_figure supplement 1D). The respiratory exchange ratio (RER) of WT mice was significantly decreased in both the light and dark phases for the first 5 days of cast immobilization, whereas similar differences were apparent only for the first 2 days in IL-6 KO mice (Figure 5_figure supplement 1E and 1F). IL-6 has been shown to promote lipolysis and fatty acid oxidation in WAT.[26] We found that, unlike in WT mice, cast immobilization did not result in a loss of eWAT mass in IL-6 KO mice (Figure 5_figure supplement 1G). Collectively, these data suggested that utilization of energy substrates was not substantially altered by cast immobilization in IL-6 KO mice.

The amounts of BCAAs in soleus were significantly increased after cast

immobilization in WT mice but not in IL-6 KO mice (Figures 5H–5J). Serum BCAA concentrations were decreased after cast immobilization in both WT and IL-6 KO mice (Figure 5_figure supplement 1H–1J). These findings suggested that deficiency of IL-6 impairs the maintenance of core body temperature and alters energy metabolism in BAT and skeletal muscle in mice subjected to cast immobilization.

Administration of IL-6 increases BCAA concentrations in skeletal muscle of cast-immobilized IL-6 KO mice

We examined whether administration of exogenous IL-6 might increase amino acid concentrations in skeletal muscle and BAT of IL-6 KO mice with cast immobilization. Administration of IL-6 restored the increase in the amounts of amino acids including BCAAs in soleus of IL-6 KO mice with cast immobilization (Figures 6A–6C and Figure 6_figure supplement 1A). Treatment with IL-6 also increased expression of *Saa3* and *Socs3* (Figure 6_figure supplement 1B and 1C) as well as the amounts of BCAAs (Figure 6D) in cultured mouse C2C12 myotubes. However, the amounts of carbohydrate metabolites in iBAT of cast-immobilized IL-6 KO mice were not increased by IL-6 administration (Figure 6_figure supplement 1D). In contrast to its effects on soleus, administration of IL-6 also did not increase the amounts of amino acids in iBAT of IL-6 KO mice with cast immobilization (Figure 6_figure supplement 1A and 1E). In addition, exogenous IL-6 did not increase the expression of UCP1, SLC25A44, and BCKDHA genes in iBAT of these mice (Figure 6_figure supplement 1F–1H). On the other hand, administration of IL-6 ameliorated the cold intolerance of IL-6 KO mice with cast immobilization (Figure 6E). We therefore examined whether IL-6 might increase core body temperature via the sympathetic nervous system with the use of C57BL/6J mice with denervated iBAT. Core body temperature of cold-exposed mice with cast immobilization and denervated iBAT was not significantly increased by administration of IL-6 (Figure 6F).

We also found that the core body temperature of IL-6 KO mice was lower than that of WT mice after cold exposure at 4°C for 4 h (Figure 6_figure supplement 1I) whereas the amount of *Ucp1* mRNA in iBAT was significantly increased for IL-6 KO mice compared with WT mice at room temperature (Figure 6_figure supplement 1J). We then investigated the possible direct effects of IL-6 on energy metabolism in BAT with the use of cultured mouse brown adipocytes. Expression of the SLC25A44, BCKDHA, and UCP1 genes in

the brown adipocytes were not increased by treatment with IL-6 (Figure 6_figure supplement 1K–1M). In contrast, treatment with the β_3-adrenergic receptor agonist CL316 243 increased the expression of these genes, and this upregulation was suppressed by treatment with IL-6 (Figure 6_figure supplement 1K–1M). Long-term administration of CL316 243 in mice was previously shown to increase expression of *Ucp1*, *Slc25a44*, and *Bckdha* in BAT.[16] We found that administration of CL316 243 for 7 days significantly increased the amounts of *Ucp1*, *Slc25a44*, and *Bckdha* mRNAs in iBAT of IL-6 KO mice but not in that of WT mice (Figure 6_figure supplement 1N–1P). Together, these data suggested that IL-6 may suppress β-adrenergic receptor–mediated thermogenesis and BCAA metabolism in brown adipocytes. Nevertheless, IL-6 induces fever response through stimulation of the central[21,22] and uptake of energy-rich BCAA delivered to BAT from skeletal muscle may facilitate a net induction of BAT thermogenesis.

Skeletal muscle–derived IL-6 increases BCAA concentrations in skeletal muscle for BAT thermogenesis

Given that our data suggested that an elevated blood concentration of IL-6 contributes to maintenance of body temperature in cast-immobilized mice in a manner dependent on the sympathetic nervous system (Figures 6E and 6F), we sought to determine the main source of circulating IL-6 in cast-immobilized mice. We first focused on the acute expression of the IL-6 gene apparent in iBAT after cast immobilization (Figure 4C), and we subjected mice to surgical removal of iBAT. The serum IL-6 concentration of such mice was not increased after cast immobilization (Figure 6G). We also found that the reduction in eWAT mass after cast immobilization in C57BL/6J mice was suppressed by surgical removal of iBAT (Figure 6H). These results suggested that BAT-derived IL-6 induces lipolysis in WAT.

We further investigated the effects of BAT-derived IL-6 on skeletal muscle. Whereas the serum concentration of IL-6 in mice depleted of iBAT was not affected by cast immobilization (Figure 6G), the concentrations of BCAAs in soleus were increased after cast immobilization in such mice (Figures 6I–6K). The amount of *Slc43a1* mRNA in soleus of mice depleted of iBAT was significantly increased by cast immobilization (Figure 6_figure supplement 2A). Gene expression for other amino acid transporters (such as SLC1A5 and SLC7A5) and for BCAA catabolic enzymes (BCAT2 and BCKDHA) in soleus also showed a similar pattern of changes after cast immobilization in iBAT-

depleted mice (Figure 6_figure supplement 2B–2E) as in intact mice (Figure 3_figure supplement 1L, 1M, 1P, and 1Q). Moreover, cast immobilization for 7 days induced similar losses of both soleus and gastrocnemius mass in mice with or without removal of iBAT (Figure 6_figure supplement 2F and Table S2). These data thus suggested that IL-6 secretion in an autocrine or paracrine manner may regulate BCAA metabolism in skeletal muscle independently of IL-6 derived from iBAT.

Acute cold exposure or restraint stress also induced IL-6 from skeletal muscle to supply BCAA for BAT thermogenesis

We further found that expression of *Il6* was also increased in not immobilized fore limb muscles (biceps brachii muscle; BBM) after cast immobilization (Figure 7_figure supplement 1A). Expression of *Saa3* and *Socs3* were increased in BBM at the same time as was that of *Il6* after cast immobilization (Figure 7_figure supplement 1B and 1C). Furthermore, gene expression for the ubiquitin ligases Atrogin-1 and MuRF-1 in BBM was increased during the early phase of cast immobilization (Figure 7_figure supplement 1D and 1E). BCAA concentrations in BBM were also increased after cast immobilization (Figure 7_figure supplement 1F-1H). These data suggest that cast immobilization stimulates BCAA metabolites in not immobilized fore limb muscles as well as immobilized muscle.

Finally, we investigated whether the thermoregulatory system through amino acid metabolism in the interaction between BAT and skeletal muscle also plays an important role in other conditions, such as cold temperature and restraint stress. Acute cold exposure increased expression of *Il6* only in iBAT and skeletal muscle in mice (Figure 7A), and expression of *Saa3* and *Socs3* were increased in soleus (Figures 7_figure supplement 1I and 1J). Gene expression for the ubiquitin ligases Atrogin-1 and MuRF-1 was not significantly increased in soleus (Figure 7_figure supplement 1K and 1L), but both soleus and gastrocnemius mass were decreased by cold exposure at 4°C for 4 h (Figure 7_figure supplement 1M and 1N). Furthermore, the amounts of valine in soleus were significantly increased by acute cold exposure in WT mice but not in IL-6 KO mice (Figures 7B-7D and Figure 7_figure supplement 1O). BCAA concentrations in soleus were also increased after cold exposure at 4°C for 4 h in iBAT-depleted mice (Figure 7_figure supplement 1P).

Restraint stress for 6 h on mice increased expression of *Ucp1* in iBAT (Figure

7_figure supplement 2A), and the amounts of *Il6* mRNA was increased in iBAT and skeletal muscle (Figures 7E and 7F). Expression of *Saa3* and *Socs3* were tended to increase in soleus (Figures 7_figure supplement 2B and 2C). Skeletal muscle mass was not decreased by restraint stress for 6 h (Figure 7_figure supplement 2D-2F), but gene expression for the ubiquitin ligases Atrogin-1 and MuRF-1 were increased after restraint stress (Figure 7_figure supplement 2G and 2H). BCAA concentrations in soleus were tended to increased by restraint stress in WT mice but not in IL-6 KO mice (Figures 7G-7I and Figure 7_figure supplement 2I). Together, thermoregulatory system through amino acid metabolism in skeletal muscle and BAT may be activated under cold temperature and acute stress.

Discussion

We have shown here that cast immobilisation leads to a passive loss of skeletal muscle function, resulting in failure to maintain adequate core body temperature in a cold environment. Cast immobilization also activated BAT thermogenesis via the sympathetic nervous system and triggered systemic changes in energy metabolism associated with BAT thermogenesis. Furthermore, we found that free BCAAs derived from skeletal muscle serve as substrates for energy metabolism in BAT, and that skeletal muscle–derived IL-6 promotes this provision of BAT with amino acids from muscle. In addition, this thermoregulatory system between BAT and skeletal muscle may also be activated in response to cold temperature or acute stress.

A first aim of our study was to investigate the role of skeletal muscle in thermogenesis. In this study, mice with impairment of hind limb muscle contraction by cast immobilization were used as a model for a loss of muscle function. Exercise-induced muscle contraction generates large amounts of heat which dependents on hydrolysis of ATP, and skeletal muscle, as the first organ to be recruited for thermogenesis, plays an important role in maintenance of body temperature in endotherms.[38] Muscle thermogenesis can account for up to 90% of systemic oxygen consumption during periods of maximal recruitment of muscle contraction, such as during exercise or an intense bout of shivering.[38,39] We found that cast immobilization decreased the amounts of metabolites in TCA cycle and suppressed expression of mitochondrial-related genes from the early stage of immobilization, suggesting that metabolic rate is rapidly decreased in immobilized muscle. On the other hands, thermoregulatory system in endotherms cannot be explained by thermogenesis based on muscle contraction alone, with nonshivering thermogenesis being required as a component of the ability to tolerate cold temperatures in the long term[1]. Our results now show that expression of the gene for sarcolipin, a key regulator of the sarco/endoplasmic reticulum Ca2+-ATPase (SERCA) and an important mediator of muscle nonshivering thermogenesis, was not increased in muscle after cast immobilization. In contrast, we have now shown that UCP3 gene expression in muscle was transiently increased during the early stage of cast immobilization. Although the importance of UCP3 for mitochondrial energy metabolism is well established,[40,41] its physiological function as a mitochondrial uncoupler remains unclear.[42,43] In addition, we found that several genes induced by cold stimulation in skeletal muscle were not increased in cast-immobilized

mice. Our results thus show that metabolic thermogenesis in skeletal muscle is crucial for mammals, and that cast immobilization increases cold intolerance, even in BAT-enriched mammals such as rodents. Although our study showed that cold intolerance in mice was observed after just 2 h of cast immobilization, these results could also be attributed not only to loss of skeletal muscle function but also to stress, decreased calorie reserves, or reduced systemic locomotor activity.

In contrast to skeletal muscle, BAT thermogenesis was activated via the sympathetic nervous system under room temperature even when skeletal muscle was immobilized. It is a well-recognized fact that BAT and skeletal muscle function in an orchestrated manner to maintain core body temperature in endotherms[5-7]. A bit surprisingly, the capacity of the BAT itself was insufficient to maintain stable body temperature during acute cold exposure. Our results also suggest that the increase in noradrenaline concentrations in BAT or in blood are transient, suggesting that the activation of sympathetic neve activity after cast immobilization is also transient. Consequently, the expression of thermogenic genes and metabolic changes in BAT may also have been induced to peak after 24 h of cast immobilization. In addition, it has been reported that long-term cast immobilization increases nonshivering thermogenesis in immobilized muscle.[44] Our results show that the expression of *Ucp2* and *Sln* were increased in immobilized muscle after 7 days of cast immobilization. These data suggest that the maintenance of core body temperature by BAT thermogenesis may be an important system during short-term cast immobilization.

We also found that changes in systemic energy metabolism induced by cast immobilization were associated with the activation of BAT thermogenesis. Activation of BAT results in the tissue becoming a high consumer of a variety of energy substrates including lipids, glucose, BCAAs, succinate, and lactate.[31] Previous findings reported that mitochondrial BCAA catabolism in brown adipocytes promotes systemic BCAA clearance, suggesting that BCAAs may be supplied to BAT from other organs during BAT thermogenesis. Our results suggest that skeletal muscle is a source of free amino acids for BAT thermogenesis or hepatic gluconeogenesis. In response to metabolic demands imposed by starvation, exercise, or cold exposure, for example, skeletal muscle manifests metabolic flexibility in order to meet the demands of other organs and is an important determinant of metabolic homeostasis.[9,10] In contrast, the

reduction in metabolic rate may contribute to protein conservation and maintain skeletal muscle mass under hibernation.[9] Our findings now provide important insight into the role of skeletal muscle as a source of amino acids. However, a recent study also suggests that a highly active proteolysis system in the heart provides substantial amounts of amino acids for distribution to other organs via the bloodstream.[45] The heart may therefore be another source of free BCAAs for BAT thermogenesis in cast-immobilized mice.

We found that muscle-derived IL-6 directly increased the abundance of BCAAs in skeletal muscle after cast immobilization. Previous studies have shown that excessive IL-6 induces amino acid catabolism in skeletal muscle,[46,47] and that IL-6 is one of the factors responsible for the induction of muscle atrophy in cast-immobilized mice.[48] IL-6 is a secreted factor induced by several mechanisms including muscle contraction, intracellular calcium signaling, and inflammation.[20,49] However, inflammation associated with macrophage infiltration is not thought to be induced in the early stages of muscle atrophy[32], and thus inflammation-induced IL-6 expression may therefore not contribute to the changes in amino acid metabolism in cast-immobilized muscle. In addition, whereas intracellular calcium concentrations may increase after muscle immobilization for 2 weeks,[44] they appear to decrease in response to short-term cast immobilization.[48] Cast immobilization induced *Il6* expression may therefore also not be regulated by calcium signaling. Upregulation of IL-6 expression by cast immobilization was previously shown to be mediated by a Piezo1-KLF15 axis,[48] whereas our observation that *Il6* expression were increased in non immobilized fore limb muscles. Furthermore, acute cold exposure and short-term restraint stress tended to increase *Il6* expression in skeletal muscle, suggesting that muscle-derived IL-6 for thermoregulatory system may also be regulated by the central nervous system. A recent study showed that motor circuits modulate the production of neutrophil-induced chemokines in skeletal muscle after acute stress.[50] The regulation of IL-6 production in muscle by the central nervous system warrants further investigation.

The central nervous system tightly controls core body temperature through integrates information about external temperature, humidity, and thermal sensation to induce an adaptive response.[1] Disappointingly, our study was inconclusive as to whether the trigger for BAT thermogenesis after cast immobilization was hypothermia associated with loss of skeletal muscle function

or stress. However, we found that acute cold exposure and short-term restraint stress may also recruits substrate supply from skeletal muscle for BAT thermogenesis. Possibly, thermoregulatory system through amino acid metabolism in skeletal muscle and BAT may also be an important metabolic strategy even in the case of fever response induced by stress or infection. Furthermore, inflammation, infection, and acute stress trigger rapid increases in the circulating IL-6 concentration[21,51] and induce a fever response by promoting PGE2 synthesis. Mitochondrial BCAA oxidation in BAT was recently shown to be increased to support thermogenesis induced by PGE2.[16] We found that BAT-derived IL-6 increased blood IL-6 levels after cast immobilization and administration of exogenous IL-6 ameliorated cold intolerance in cast-immobilized IL-6 KO mice via the sympathetic nervous system. It may modulate thermal and energy homeostasis through the fever response and metabolic regulation in multiple organs.

In conclusion, we have shown that cast immobilization induced thermogenesis in BAT that was dependent on the utilization of free amino acids derived from skeletal muscle, and that muscle-derived IL-6 stimulated BCAA metabolism in skeletal muscle. Although some effects, such as activation of BAT thermogenesis and changes in energy metabolic dynamics, observed with cast immobilization were modest in magnitude, thermoregulatory system through amino acid metabolism in skeletal muscle and BAT may be an important metabolic strategy even under cold temperature or acute stress. Our findings may provide new insights into the significance of skeletal muscle as a large reservoir of amino acids in the regulation of body temperature. In addition, given that circulating levels of IL-6 or BCAAs are associated with obesity and diabetes,[52.53] IL-6–mediated BCAA metabolism in skeletal muscle and BAT may also be associated with muscle atrophy in metabolic diseases. Further investigation of IL-6–dependent amino acid metabolism in BAT and skeletal muscle may inform the development of preventive or therapeutic interventions for some forms of muscle atrophy.

Limitations of the study

In our cast immobilization strategy, we were unable to determine which components of muscle thermogenesis are actually inhibited by cast immobilization, and what is the relative heat contribution. This study does not experiment that directly test whether BCAAs derived from adipose tissue are

used for thermogenesis, which would require more robust tracing experiments. In addition, given that rodents are BAT-enriched mammals, whether BAT thermogenesis is similarly activated in humans after skeletal muscle immobilization remains to be investigated. Our study also did not determine the mechanism underlying the induction of *Il6* expression in skeletal muscle by cast immobilization. In addition, whereas muscle-derived IL-6 may stimulate protein catabolism in immobilized muscle, the mechanism by which IL-6 increases BCAA concentrations in skeletal muscle remains unclear. In further investigation, RNA-seq profiling of BAT and muscle tissues should be used to rigorously determine the mechanisms of BCAA metabolism stimulated by muscle-derived IL-6.

Methods

Mice

All experiments were approved by the Animal Care and Use Committee of Tokushima University and were conducted in accordance with the guidelines for the care and use of animals approved by the Council of the Physiological Society of Japan. Every effort was made to minimize animal suffering and to reduce the number of animals used in the experiments. All mice were housed at a constant room temperature of 23° ± 1°C and with a 12-h-light/12-h-dark cycle (lights on at 8.00 a.m.). They were fed standard nonpurified chow (Oriental Yeast) and had free access to both food and water. Our study examined male mice because male animals exhibited less variability in phenotype. Male mice at 9 to 13 weeks of age were studied. The mice were randomly assigned to experimental groups at the time of purchase or weaning. C57BL/6J mice were obtained from Japan SLC (Shizuoka, Japan), and IL-6 KO mice (B6;129S2-Il6<tm1kopf>) from RIKEN BRC through the National Bioresource Project of MEXT/AMED.[52] The IL-6 KO mice were maintained on the C57BL/6J background.

Cells

The mouse myoblast cell line C2C12 was obtained from American Type Culture Collection (CRL-1772™) and was maintained in Dulbecco's modified Eagle's medium (DMEM) containing 25 mM glucose (#D6429, Sigma) and supplemented with 10% fetal bovine serum (535-94155, BioSera) and 1% penicillin-streptomycin (15140-122, Gibco). After the cells had achieved 95% to 100% confluence, the culture medium was changed to DMEM containing 25 mM glucose and supplemented with 2% horse serum (16050-130, Thermo Fisher Scientific) and the cells were cultured for 5 days to promote their differentiation from myoblasts into myotubes. The myotubes were washed with phosphate-buffered saline (PBS) and then incubated in DMEM containing 25 mM glucose and supplemented with 1% bovine serum albumin (A8806-5G, Sigma) and 1% penicillin-streptomycin for 16 h before exposure to recombinant mouse IL-6 (rIL-6) at 50 ng/ml (575702, BioLegend) or vehicle (PBS) in the same medium for 1 h. The treated cells were washed with PBS or 5% mannitol solution and collected for RNA or metabolite extraction.

Mouse preadipocytes were obtained from Dr. Takeshi Yoneshiro the University of Tohoku, Tohoku, Japan[54] and were maintained in DMEM

containing 25 mM glucose and supplemented with 10% fetal bovine serum and 1% penicillin-streptomycin. After the cells had achieved 95% to 100% confluence, they were induced to differentiate into brown adipocytes by incubation in the same medium that was also supplemented with 1 nM triiodothyronine (45006-44, Nacalai Tesque), insulin (093-06473, Wako) at 5 µg/ml, dexamethasone (11107-51, Nacalai Tesque) at 2 µg/ml, 0.5 mM isobutylmethylxanthine (15879, Sigma), and 125 µM indomethacin (19233-51, Nacalai Tesque). After culture for 2 days, the medium was replaced with DMEM containing 25 mM glucose and supplemented with 10% fetal bovine serum, 1% penicillin-streptomycin, and insulin (5 µg/ml), and the cells were maintained in this medium with medium replenishment every 2 days. The cells were fully differentiated at 6 to 7 days after the induction of differentiation. For experiments, the brown adipocytes were washed with PBS at 7 days after differentiation initiation and then incubated in DMEM containing 25 mM glucose and supplemented with 1% bovine serum albumin and 1% penicillin-streptomycin for 12 h before exposure to rIL-6 (50 ng/ml), 1 µM CL316 243 (Ab144605, Abcam), both agents, or vehicle (PBS). The treated cells were collected after 24 h for RNA extraction.

Cast immobilization

Mice were subjected to bilateral or unilateral cast immobilization of hind limbs, and unfixed mice were studied as controls. In brief, mice were lightly anesthetized with inhalational isoflurane (MSD Animal Health), and the hind limbs were fixed in a natural position, with care taken to avoid skin irritation and congestion. After casting, the mice were housed individually with free access to standard mouse chow and water. The mice out of cast immobilization were excluded from experiments. In all experiments, mice were killed by cardiac puncture after food deprivation for 3 h and tissue samples were collected. Proportion of immobilized skeletal muscle weight for cast-immobilized mice was obtained by extirpation skeletal muscle of the posterior cervical region and measuring wet tissue weights.

Surgical denervation of iBAT

Surgical denervation of iBAT was performed on 9-week-old male mice as described previously.[55] Animals were anesthetized by intraperitoneal injection of domitor (Zenoaq) at a dose of 0.75 mg/kg, midazolam (Wako) at 4 mg/kg, and

butorphanol tartrate (Meiji Seika Pharma) at 5 mg/kg, and the incision site was shaved and then disinfected with 0.05% chlorhexidine gluconate (5% Hibitane, Sumitomo Pharma). A midline skin incision was made in the interscapular region to expose both iBAT pads, the nerve fibers (five nerves per pad) were identified and cut with sterile scissors, and the incision was closed with sutures. For sham surgery, a skin incision was made and the medial side was gently exposed. All mice were then individually housed in clean cages at room temperature and were monitored daily. Cast immobilization was performed 1 week after surgery.

Surgical removal of iBAT

Surgical removal of iBAT was performed on 11-week-old male mice, with cast immobilization being performed 1 week after surgery. Animals were anesthetized and the incision site was shaved and disinfected as described for iBAT denervation. A midline skin incision was made in the interscapular region, all iBAT was removed, and the incision was closed with sutures. For sham surgery, a skin incision was made and the medial side was gently exposed. All mice were then housed individually in clean cages at room temperature.

Acute cold tolerance test

Core body temperature was measured with a Homeothermic Monitor (BWT-100A, BRC) by gentle insertion of a thermal probe into the rectum of the mouse. After recording of baseline body temperature at room temperature, animals were placed in a cold chamber at 4°C for up to 4 h without access to food. Tissue was then collected and snap-frozen.

Acute Restraint Stress

Mice were confined in 50-mL tubes with several ventilation holes of about 0.5 cm in diameter on the sides, and were restrained for 6 hours without access to food. Mice restrained in tubes were maintained in a state in which they could hardly move their bodies. In all experiments, mice were killed by cardiac puncture and tissue samples were collected.

Treatment of mice with CL316 243 or rIL-6

IL-6 KO mice with cast immobilization for 24 h were subjected to intraperitoneal administration of 400 ng of rIL-6 (575702, BioLegend) in saline or of saline

alone. The mice were maintained sedentary for 3 h without access to food before collection of tissue samples. Acute exposure to a cold environment chamber was initiated 30 min after intraperitoneal treatment with rIL-6 (400 ng) or saline in IL-6 KO mice or in C57BL/6J mice with denervated iBAT that had been subjected to cast immobilization for 24 h. IL-6 KO mice with denervated iBAT were treated intraperitoneally with CL316 243 (Ab144605, Abcam) at a dose of 0.1 mg/kg, rIL-6 (400 ng), both agents, or saline vehicle, and tissue was collected 3 h later. For long-term treatment of IL-6 KO mice with CL316 243, the animals were injected intraperitoneally with the drug (0.1 mg/kg per day) or saline for 7 days. Tissue was collected at 3 h after drug treatment on the last day.

Oxygen consumption and RER measurement

Mice were acclimated to the analysis cage for 3 days before the start of metabolic measurements. They were housed individually with free access to food and water. Analysis of respiratory gases was performed with a mass spectrometer (ARCO-2000, ARCO System). Measurements were performed for seven consecutive days after cast immobilization.

Locomotor activity recording

The activity level of mice was assessed with an infrared activity monitor (ACTIMO-100N, Shin Factory). A cage containing one mouse was placed inside the activity monitor with infrared beams at 20-mm intervals. Mouse movements were counted every 0.5 s for 24 h. Recording was performed for seven consecutive days after cast immobilization.

RNA isolation and RT and real-time PCR analysis

Total RNA was extracted from mouse tissues and cells with the use of RNAiso (#9109, Takara Bio) and subjected to RT with the use of a TaKaRa PrimeScript II 1st Stand cDNA Synthesis Kit (Takara Bio). The resulting cDNA was subjected to real-time PCR analysis with Fast SYBR Green Master Mix (3485612, Applied Biosystems) in a Step One Plus Real-Time PCR System (Applied Biosystems). The abundance of target mRNAs was normalized by that of *Gapdh* mRNA. The PCR primers are listed in Table S3.

Protein extraction and immunoblot analysis

Total protein was extracted from mouse tissues by homogenization in a lysis solution consisting of 1 M Tris-HCL (pH 7.4), 0.1 M EDTA, 1% Nonidet P-40, 5 mM sodium pyrophosphate, and phosphatase (25955-24, Nacalai Tesque) and protease (07575-51, Nacalai Tesque) inhibitor cocktails. The homogenate was centrifuged at 15,000 $\times$ *g* for 15 min at 4°C, and the resulting supernatant was assayed for protein concentration with a Pierce BCA Protein Assay Kit (Thermo Fisher Scientific) and then subjected to SDS-polyacrylamide gel electrophoresis on a 10% acrylamide/4% bisacrylamide gel. The separated proteins were transferred to polyvinylidene difluoride membrane, which was then exposed to 5% dried skim milk for 1 h at room temperature before incubation with primary antibodies including those to PGC-1α (A12348, Abclonal), to UCP1 (sc-293418, Santa Cruz Biotechnology), and to GAPDH (CAB932Hu01, Cloud-Clone) for 16 h at 4°C. Immune complexes were detected with horseradish peroxidase–conjugated secondary antibodies (458, MBL; 7076P2, Cell Signaling Technology), enhanced chemiluminescence reagents (170-5061, Bio-Rad Labotatories, Inc.), and an Amersham Imager 600 instrument (GE Healthcare). Band intensity was quantified with ImageJ software.

Histology

BAT was fixed in formalin, sectioned, and stained with hematoxylin-eosin.

Metabolomics analysis

Targeted profiling of amino acid metabolites was performed by capillary electrophoresis–time-of-flight mass spectrometry (CE-TOF/MS) with an Agilent 7100 CE system coupled to an Agilent 6230 TOF mass spectrometer (Agilent Technologies) according to previously described methods.[30] The collected metabolite data were subjected to enrichment analysis using Metaboanalyst 6.0 (https://www.metaboanalyst.ca). Pathway enrichment was tested using the SMPDB databases.

Measurement of noradrenaline

Tissue samples were homogenized in methanol containing internal standards ((±)-Norepinephrine-D6 hydrochloride solution, Sigma-Ardrich). The mixture was centrifuged at 4 °C, and the aqueous fraction was isolated and centrifuged through an cosmonice filter W (06543-04, nacalai tesque). Noradrenaline content of the supernatants was measured by high-performance liquid

chromatography (SHIMAZU) with a reversed-phase column (Cadenza CD-C18 MF 100×2 mm 3 μm, Imtakt) and tandem mass spectrometry (MS/MS) (API 3200, AB SCIEX). Data are analyzed using AnalystLauncher (AB SCIEX).

Measurement of [^{3}H]leucine uptake

Mice were deprived of food for 3 h before intravenous injection of L-[4,5-^{3}H(*N*)]leucine (NET1166, PerkinElmer) at a dose of 1 μCi/g. They were then maintained in a resting state for 40 min until blood and tissue collection, with perfusion being performed before tissue isolation. Isolated tissue was cut into small pieces, which were then placed in a round-bottom polypropylene tube before the addition of 500 μl of distilled water, 150 μl of 30% hydrogen peroxide (Wako), and 150 μl of 2 M KOH (1310-58-3, Hayashi Pure Chemical) in 2-propanol (000-64783, Kishida Chemical) and incubation at 65°C for 2 h. The tissue lysate was neutralized with 30% acetic acid, and 1 ml of liquid scintillation solubilizer (Soluen-350, PerkinElmer) was added to the sample before incubation at 50°C for 5 h and the further addition of 5 ml of liquid scintillation cocktail (Hionic-Flour, PerkinElmer). Leucine uptake in each organ was quantified by measurement of radioactivity with a scintillation counter (LSC-7400, Hitachi).

Hepatic glycogen assay

The liver was homogenized in ice-cold citrate buffer (pH 4.2) containing NaF (2.5 g/l), the homogenate was centrifuged at 14,000 × *g* for 5 min at 4°C, and the resulting supernatant was assayed for glycogen with an EnzyChrom Glycogen Assay Kit (BioAssay Systems).

ELISAs

Blood samples were collected from the heart of mice that had been anesthetized by intraperitoneal injection of domitor (Zenoaq) at a dose of 0.75 mg/kg, midazolam (Wako) at 4 mg/kg, and butorphanol tartrate (Meiji Seika Pharma) at 5 mg/kg after food deprivation for 3 h, and they were centrifuged at 7500 × *g* for 10 min at 4°C to isolate serum. Serum IL-6 and TNF-α concentrations were determined with enzyme-linked immunosorbent assay (ELISA) kits (Legend Max Mouse IL-6 ELISA Kit, BioLegend, and Mouse TNF Alpha Uncoated ELISA, Invitrogen, respectively). Serum noradrenaline was extracted with the use of a cis-diol–specific affinity gel, acylated, enzymatically

converted, and then measured with an ELISA kit (Noradrenaline Research ELISA, ImmuSmol). Serum corticosterone was determined with a Corticosterone ELISA Kit (Enzo Life Sciences).

Statistical analysis

Data are presented as means ± SEM unless indicated otherwise and were analyzed with statistical software (JMP or Statcel–The Useful Add-in Forms on Excel 4th ed.). Comparisons between two groups were performed with the paired or unpaired t test, as appropriate. Those among more than two groups were performed with Dunnett's test, by one-way analysis of variance (ANOVA) followed by the Tukey-Kramer test, or by two-way ANOVA followed by Tukey's post hoc test or the post hoc paired/unpaired t test with Bonferroni's correction. A two-tailed p value was calculated for all experiments, and a value of <0.05 was considered statistically significant.

Acknowledgements

We thank members of the Radioisotope Center of Tokushima University Graduate School for technical support with the tracer experiments; members of the Special Mission Center for Metabolome Analysis, School of Medical Nutrition, Faculty of Medicine, Tokushima University, for technical support with the metabolomics analysis; Yoichiro Iwakura (University of Tokyo) for permission to study the IL-6 KO mice; Kohta Onishi (University of Tokushima) for technical support with the LC/MS/MS analysis; and the Support Center for Advanced Medical Sciences at Tokushima University Graduate School of Biomedical Sciences for general technical support. This study was supported by Funds for the Development of Human Resources in Science and Technology from the Ministry of Education, Culture, Sports, Science, and Technology of Japan (MEXT) through the Home for Innovative Researchers and Academic Knowledge Users consortium, and by KAKENHI grants (21J14844 to Y.I.-M., 23K19926 to Y.I.-M., 22H03535 to H.S., and 21K11724 to R.T.) from the Japan Society for the Promotion of Science.

Auther Contributions

Y.I.-M., T.S., S.F., M.T., M.S. and M.T. conducted the experiments; R.T. and H.S. designed the experiments; Y.I.-M., R.T., and H.S. wrote the manuscript; Y.O.-O., T.Y., K.N., and M.K. provided conceptual advice on data interpretation.

Decompeting interests

The authors declare no competing interests.

Correspondence and requests for materials should be addressed to Hitoshi Sakaue.

References

1. Tansey, E.A., Johnson, C.D. (2015) Recent advances in thermoregulation. Adv Physiol Educ. 39 (3):139-48
https://doi.org/10.1152/advan.00126.2014

2. Piscitiello, E., Herwig, A., Haugg, E., Schröder, B., Breves G., *et al*. (2021) Acclimation of intestinal morphology and function in Djungarian hamsters (Phodopus sungorus) related to seasonal and acute energy balance. J Exp Biol. 16;224(Pt 4): jeb232876
https://doi.org/10.1242/jeb.232876

3. Cannon, B., Nedergaard, J. (2004) Brown adipose tissue: function and physiological significance. Physiol Rev. 84(1): 277-359
https://doi.org/10.1152/physrev.00015.2003

4. Nowack, J., Giroud, S., Arnold, W., Ruf, T. (2017) Muscle Non-shivering Thermogenesis and Its Role in the Evolution of Endothermy. Front Physiol. 8: 889
https://doi.org/10.3389/fphys.2017.00889

5. Rowland, L. A., Bal, N. C., Kozak,L. P., Periasamy, M. (2015) Uncoupling Protein 1 and Sarcolipin Are Required to Maintain Optimal Thermogenesis, and Loss of Both Systems Compromises Survival of Mice under Cold Stress. J Biol Chem. 8;290(19):12282-9
https://doi.org/10.1074/jbc.M115.637603

6. Golozoubova, V., Hohtola, E., Matthias, A., Jacobsson, A., Cannon, B., Nedergaard, J. (2001) Only UCP1 can mediate adaptive nonshivering thermogenesis in the cold. FASEB J. 15(11):2048-50
https://doi.org/10.1096/fj.00-0536fje

7. Janovska, P., Zouhar, P., Bardova, K., Otahal, J., Vrbacky, M., *et al*. (2013) Impairment of adrenergically-regulated thermogenesis in brown fat of obesity-resistant mice is compensated by non-shivering thermogenesis in skeletal muscle. Mol Metab. 69:101683
https://doi.org/10.1016/j.molmet.2023.101683

8. Blondin, D.P., Frisch, F., Phoenix, S., Guérin, B., Turcotte, É. E., *et al*. (2017) Inhibition of Intracellular Triglyceride Lipolysis Suppresses Cold-Induced Brown Adipose Tissue Metabolism and Increases Shivering in Humans. Cell Metab. 25(2): 438-447
https://doi.org/10.1016/j.cmet.2016.12.005

9. Bertile, F., Habold, C., Maho, Y. L., Giroud, S. (2021) Body Protein Sparing in Hibernators: A Source for Biomedical Innovation. Front Physiol. 18:12:634953
https://doi.org/10.3389/fphys.2021.634953

10. Holeček, M. (2018) Branched-chain amino acids in health and disease: metabolism, alterations in blood plasma, and as supplements. Nutr Metab (Lond). 15:33
https://doi.org/10.1186/s12986-018-0271-1

11. Heine, M., Fischer, A.W., Schlein, C., Jung, C., Straub, L.G., *et al*. (2018) Lipolysis Triggers a Systemic Insulin Response Essential for Efficient Energy Replenishment of Activated Brown Adipose Tissue in Mice
Cell Metab. 28(4): 644-655.e4
https://doi.org/10.1016/j.cmet.2018.06.020

12. Padmini, P., Khedoe, S.J., Hoeke, G., Kooijman, S., Dijk, W. *et al*. (2015) Brown adipose tissue takes up plasma triglycerides mostly after lipolysis. J Lipid Res. 56(1): 51-9
https://doi.org/10.1194/jlr.M052746

13. Olsen, J.S., Aslund, A., Bokhari, M.H., Hutchison, D.S., Bengtsson, T. (2019) Acute β-adrenoceptor mediated glucose clearance in brown adipose tissue; a distinct pathway independent of functional insulin signaling. Mol Metab. 30:240-249
https://doi.org/10.1016/j.molmet.2019.10.004

14. Millis, E.L., Pierce, K.A., Jedrychowski, M.P., Garrity, R., Winther, S. *et al*. (2018) Accumulation of succinate controls activation of adipose tissue thermogenesis. Nature. 560(7716): 102-106

https://doi.org/10.1038/s41586-018-0353-2

15. Yoneshiro, T., Wang, Q., Tajima, K., Matsushita, M., Maki, H., *et al*. (2019) BCAA catabolism in brown fat controls energy homeostasis through SLC25A44. Nature. 572(7771): 614-619
https://doi.org/10.1038/s41586-019-1503-x

16. Yoneshiro, T., Kataoka, N., Walejko, J.M., Ikeda, K., Brown, Z. *et al*. (2021) Metabolic flexibility via mitochondrial BCAA carrier SLC25A44 is required for optimal fever. Elife. 10: e66865
https://doi.org/10.7554/elife.66865

17. Reddy, A., Bozi, L.H.M., Yaghi, O.K., Millis, E.L., Xiao, H., *et al*. (2020) pH-Gated Succinate Secretion Regulates Muscle Remodeling in Response to Exercise. Cell. 183(1):62-75. e17
https://doi.org/10.1016/j.cell.2020.08.039

18. de Oliveira Dos Santos A.R. de Oliveira Zanuso B. Miola V.F.B. *et al*. (2021) Adipokines, Myokines, and Hepatokines: Crosstalk and Metabolic Repercussions. Int J Mol Sci. 22(5): 2639
https://doi.org/10.3390/ijms22052639

19. Tanaka, T., Narazaki, M., Kishimoto, T. (2014) IL-6 in inflammation, immunity, and disease. Cold Spring Harb Perspect Biol. 6(10): a016295
https://doi.org/10.3390/ijms22052639

20. Pedersen, B.K., Febbraio, M.A. (2008) Muscle as an Endocrine Organ: Focus on Muscle-Derived Interleukin-6. Physiol Rev. 88(4): 1379-406
https://doi.org/10.1152/physrev.90100.2007

21. Qing, H., Desrouleaux, R., Israni-Winger, K., Mineur, Y.S., Fogelman, N., *et al*. (2020) Origin and Function of Stress-Induced IL-6 in Murine Models. Cell. 182(2): 372-387.e14
https://doi.org/10.1016/j.cell.2020.05.054

22. Chen, Q., Wang, W. C., Bruce, R., Li, H., Schleider, D.M., Mulbury, M.J. *et al*.

(2004) Central role of IL-6 receptor signal-transducing chain gp130 in activation of L-selectin adhesion by fever-range thermal stress. Immunity. 20(1): 59-70 https://doi.org/10.1016/s1074-7613(03)00358-3

23. Serrano, A. L., Baeza-Raja, B., Perdiguero, E., Muñoz-Cánoves, M.P. (2008) Interleukin-6 Is an Essential Regulator of Satellite Cell-Mediated Skeletal Muscle Hypertrophy. Cell Metab. 7(1): 33-44 https://doi.org/10.1016/j.cmet.2007.11.011

24. Ellingsgaard, H., Hauselmann, I., Schuler, B., Habib, A.M., Baggio, L.L., *et al*. (2011) Interleukin-6 enhances insulin secretion by increasing glucagon-like peptide-1 secretion from L cells and alpha cells. Nat Med. 17(11): 1481-9 https://doi.org/10.1038/nm.2513

25. Knudsen, J. G., Murholm, M., Carey, A.L., Beins, R.S., Basse, A.L.,et al. (2014) Role of IL-6 in exercise training- and cold-induced UCP1 expression in subcutaneous white adipose tissue. PLoS One. 9(1): e84910 https://doi.org/10.1371/journal.pone.0084910

26. Hall, G. V., Steensberg, A., Sacchetti, M., Fischer, C., Keller, C., *et al*. (2003) Interleukin-6 stimulates lipolysis and fat oxidation in humans. J Clin Endocrinol Metab. 88(7): 3005-10 https://doi.org/10.1210/jc.2002-021687

27. Nonogaki, K., Fuller, G.M., Fuentes, N.L., Moser, A.H., Staprans, I., *et al*. (1995) Interleukin-6 stimulates hepatic triglyceride secretion in rats. Endocrinology. 136(5): 2143-9 https://doi.org/10.1210/endo.136.5.7720663

28. Maurya S.K. Herrera J.L. Sahoo S.K. Reis F.C.G. Vega R.B. Kelly D.P. Periasamy M. (2018). Sarcolipin Signaling Promotes Mitochondrial Biogenesis and Oxidative Metabolism in Skeletal Muscle. Cell Rep. 24(11): 2919-2931. https://doi.org/10.1016/j.celrep.2018.08.036.

29. Bartness, T.J., Vaughan, C.H., Song, C.K. (2010) Sympathetic and sensory innervation of brown adipose tissue. Int J Obes (Lond). 34 Suppl 1(0 1): S36-42

https://doi.org/10.1038/ijo.2010.182

30. Okamatsu-Ogura, Y., Kuroda, M., Tsutsumi, R., Tsubota, A., Saito, M., *et al*. (2020) UCP1-dependent and UCP1-independent metabolic changes induced by acute cold exposure in brown adipose tissue of mice. Metabolism. 113: 154396 https://doi.org/10.1016/j.metabol.2020.154396

31. Wang, Z., Wang, Q.A., Liu, Y., Jiang, L. (2021) Energy metabolism in brown adipose tissue. FEBS J. 288(12): 3647-3662 https://doi.org/10.1111/febs.16015

32. Kawanishi, N., Funakoshi, T., Machida, S. (2018) Time-course study of macrophage infiltration and inflammation in cast immobilization-induced atrophied muscle of mice. Muscle Nerve. 57(6): 1006-1013 https://doi.org/10.1002/mus.26061

33. Gazzola, R.F., Sala, R., Bussolati, O., Visigalli, R., Dall'Asta, V., *et al*. (2001) The adaptive regulation of amino acid transport system A is associated to changes in ATA2 expression. FEBS Lett. 490(1-2): 11-4 https://doi.org/10.1016/s0014-5793(01)02126-3

34. Gjymishka, A., Palii, S.S., Shan, J., Kilberg, M.S. (2008) Despite increased ATF4 binding at the C/EBP-ATF composite site following activation of the unfolded protein response, system A transporter 2 (SNAT2) transcription activity is repressed in HepG2 cells. J Biol Chem. 283(41): 27736-27747 https://doi.org/10.1074/jbc.m803781200

35. HUANG, Y. and CHUANG, D.T. (1999) Down-regulation of rat mitochondrial branched-chain 2-oxoacid dehydrogenase kinase gene expression by glucocorticoids. Biochem. J. 339: 503–510

36. Kobayashi, R., Shimomura, Y., Murakami, T., Nakai, N., Otsuka, M., *et al*. (1999) Hepatic branched-chain α-keto acid dehydrogenase complex in female rats: activation by exercise and starvation. J Nutr Sci Vitaminol 45: 303-9 https://doi.org/10.3177/jnsv.45.303

37. Fukuhara, D., Kanai, Y., Chairoungdua, A., Babu, E., Bessho, F., *et al*. (2007) Protein characterization of Na+-independent system l amino acid transporter 3 in mice: a potential role in supply of branched-chain amino acids under nutrient starvation. Am. J. Pathol. 170 (3): 888-89 https://doi.org/10.2353/ajpath.2007.060428

38. Rowland, L.A., Bal, N.C., Periasamy, M. (2015) The role of skeletal-muscle-based thermogenic mechanisms in vertebrate endothermy. Biol Rev Camb Philos Soc. 90(4): 1279-97 https://doi.org/10.1111/brv.12157

39. Zurlo, F., Larson, K., Bogardus, C., Ravussin, E. (1990) Skeletal muscle metabolism is a major determinant of resting energy expenditure. J Clin Invest. 86(5): 1423-7 https://doi.org/10.1172/jci114857

40. Bouillaud F. Alves-Guerra M. Ricquier D. (2016). UCPs, at the interface between bioenergetics and metabolism. Biochim Biophys Acta. 1863(10): 2443-56. https://doi.org/10.1016/j.bbamcr.2016.04.013

41. Lombardi A. Busiello R.A. Matteis R.D. Lionetti L. Savarese S. Moreno M. Gentile A. Silvestri E. Senese R. Lange P.D. Cioffi F. Lanni A. Goglia F. (2019). Absence of Uncoupling Protein-3 at Thermoneutrality Impacts Lipid Handling and Energy Homeostasis in Mice. Cells. 8(8): 916. https://doi.org/10.3390/cells8080916.

42. Vidal-Puig A.J. Grujic D. Zhang C.Y. Hagen T. Boss O. Ido Y. Szczepanik A. Wade J. Mootha V. Cortright R. Muoio D.M. Lowell B.B. (2000). Energy metabolism in uncoupling protein 3 gene knockout mice. J Biol Chem. 275(21): 16258-66. https://doi.org/10.1074/jbc.M910179199.

43. Shabalina I.G. Hoeks J. Kramarova T.V. Schrauwen P. Cannon B. Nedergaard J. (2010). Cold tolerance of UCP1-ablated mice: a skeletal muscle mitochondria switch toward lipid oxidation with marked UCP3 up-regulation not associated with increased basal, fatty acid- or ROS-induced uncoupling or enhanced GDP effects. Biochim Biophys Acta. 1797(6-7): 968-80.

https://doi.org/10.1016/j.bbabio.2010.02.033.

44. Tomiya, S., Tamura, Y., Kouzaki, K., Kotani, T., Wakabayashi, Y., *et al*. (2019) Cast immobilization of hindlimb upregulates sarcolipin expression in atrophied skeletal muscles and increases thermogenesis in C57BL/6J mice. Am J Physiol Regul Integr Comp Physiol. 317(5): R649-R661
https://doi.org/10.1152/ajpregu.00118.2019

45. Murashige, D., Jang, C., Neinast, M., Edwards, J.J., Cowan, A., *et al*. (2020) Comprehensive quantification of fuel use by the failing and nonfailing human heart. Science. 370(6514): 364-368
https://doi.org/10.1126/science.abc8861

46. Bonetto, A., Aydogdu, T., Jin, X., Zhang, Z., Zhan, R.,*et al*. (2012) JAK/STAT3 pathway inhibition blocks skeletal muscle wasting downstream of IL-6 and in experimental cancer cachexia. Am J Physiol Endocrinol Metab 303: E410–E421
https://doi.org/10.1152/ajpendo.00039.2012

47. Zanders, L., Kny, M., Hahn, A., Schmidt, S., Wundersitz, S., *et al*. (2022) Sepsis induces interleukin 6, gp130/JAK2/STAT3, and muscle wasting. J Cachexia Sarcopenia Muscle. 2022; 13(1): 713-727
https://doi.org/10.1002/jcsm.12867

48. Hirata, Y., Nomura, K., Kato, D., Tachibana, Y., Niikura, T., *et al*. (2022) A Piezo1/KLF15/IL-6 axis mediates immobilization-induced muscle atrophy. J Clin Invest. 132(10): 1-13
https://doi.org/10.1172/jci154611

49. Bustamante, M., Fernández-Verdejo, R., Jaimovich, E., Buvinic, S. (2014) Electrical stimulation induces IL-6 in skeletal muscle through extracellular ATP by activating Ca (2+) signals and an IL-6 autocrine loop. Am J Physiol Endocrinol Metab. 306(8): E869-82
https://doi.org/10.1152/ajpendo.00450.2013

50. Poller, W.C., Downey, J., Mooslechner, A.A., Khan, N., Li, L., *et al*. (2022)

Brain motor and fear circuits regulate leukocytes during acute stress. Nature. 607(7919): 578-584
https://doi.org/10.1038/s41586-022-04890-z

51. Cheng, Y., Jope, R.S., Beurel, E. (2015) A pre-conditioning stress accelerates increases in mouse plasma inflammatory cytokines induced by stress. BMC Neurosci. 16:31
https://doi.org/10.1186/s12868-015-0169-z

52. Wallenius, V., Wallenius, K., Ahrén, B., Rudling, M., Carlsten, H., *et al*. (2002) Interleukin-6-deficient mice develop mature-onset obesity. Nat Med. 8(1): 75-9
https://doi.org/10.1038/nm0102-75

53. Wang, T.J., Larson, M.G., Vasan, R.S., Cheng, S., Rhee, E.P. *et al*. (2011) Metabolite profiles and the risk of developing diabetes. Nat Med. 17(4): 448-53
https://doi.org/10.1038/nm.2307

54. Shinoda, K., Luijten, I.H.N., Hasegawa, Y., Hong, H., Sonne, S.B., *et al*. (2015) Genetic and functional characterization of clonally derived adult human brown adipocytes. Nat Med. 21(4):389-94
https://doi.org/10.1038/nm.3819

55. Vaughan, C.H., Zarebidaki, E., Ehlen, J.C., Bartness, T.J. (2014) Analysis and measurement of the sympathetic and sensory innervation of white and brown adipose tissue. Methods Enzymol. 537: 199-225
https://doi.org/10.1016/b978-0-12-411619-1.00011-2

Figure Legends

Figure 1. Cast immobilization induces BAT thermogenesis via sympathetic activation

(A) Time course of rectal core body temperature of cast-immobilized (gypsum, n = 6) and control (n = 5) mice subjected to a cold (4°C) challenge test. The test was performed 7 days after bilateral immobilization of hind limbs.

(B) Rectal core body temperature of cast-immobilized (n = 5) and control (n = 5) mice during cold (4°C) exposure at 24 h after bilateral cast immobilization.

(C) Decline in rectal temperature of cast-immobilized and control (n = 9) mice after cold (4°C) exposure for 4 h performed 2 h after unilateral (UL, n =8) or bilateral (BL, n = 9) immobilization.

(D) Reverse transcription (RT) and real-time polymerase chain reaction (PCR) analysis of the *Ucp1/Gapdh* mRNA abundance ratio in iBAT of control mice and mice subjected to bilateral cast immobilization for the indicated times (n = 7 to 13 per group).

(E–G) Immunoblot analysis of PGC-1α (n = 3 or 4 per group) and UCP1 (n = 6 per group) in iBAT of control mice and mice subjected to bilateral cast immobilization for the indicated times. GAPDH was examined as a loading control. Representative blots (E) and densitometric quantitation of the PGC-1α/GAPDH (F) and UCP1/GAPDH (G) band intensity ratios are shown.

(H) Noradrenaline concentrations in iBAT of cast-immobilized (n = 4) and control (n = 4) mice after subsequent biteral cast immobilization.

(I) RT and real-time PCR analysis of the *Ucp1/Gapdh* mRNA abundance ratio in iBAT subjected to surgical denervation or sham surgery, either in control mice or in mice at 24 h after subsequent bilateral cast immobilization (n = 6–9 per group).

(J) Rectal core body temperature of mice as in (I) subjected to cold (4°C) exposure for 1 h (n = 3 or 4 per group).

All quantitative data are means ± SEM. *$p < 0.05$, **$p < 0.01$ as determined by two-way ANOVA followed by Tukey's post hoc test or the post hoc paired/unpaired t test with Bonferroni's correction (A, B, I and J), by one-way ANOVA followed by Tukey's post hoc test (C), by Dunnett's test (D, F, G and H), or by the unpaired t test (I).

See also Figure 1_figure supplement 1 and 2, and Table S1.

Figure 2. Cast immobilization alters systemic metabolic dynamics associated with BAT thermogenesis

(A and B) Concentrations of carbohydrate metabolites (A) and amino acids (B) in sham-operated or denervated iBAT of mice without (control) or at the indicated times after bilateral cast immobilization. The metabolomics data are presented as heat maps corresponding to the $\log_{10}$ value of fold change in cast-immobilized mice relative to the corresponding control mice and are means of four or five mice in each group. TCA, tricarboxylic acid cycle.

(C and D) RT and real-time PCR analysis of mRNA abundance for the fatty acid transporter CD36 and the succinate transporter SLC25A10 in sham-operated or denervated iBAT of control mice or mice subjected to bilateral cast immobilization for 24 h (n = 6 per group).

(E) Succinate content of sham-operated or denervated iBAT of control mice or mice subjected to bilateral cast immobilization for 24 h (n = 3–5 per group).

(F and G) Oxygen consumption rate (VO_2) and respiratory exchange ratio (RER), respectively, for control mice and mice subjected to bilateral cast immobilization for 7 days (n = 6 per group).

(H) Weight of eWAT for control mice and mice subjected to bilateral cast immobilization for the indicated times (n = 5–7 per group).

(I) Hepatic glycogen content for control mice and mice subjected to bilateral cast immobilization for the indicated times (n = 6–10 per group).

Date in (C) through (I) are means ± SEM. *$p < 0.05$, **$p < 0.01$ as determined by one-way ANOVA followed by Tukey's post hoc test (C–E), by two-way ANOVA followed by Tukey's post hoc test or the unpaired post hoc t test with Bonferroni's correction (F and G), or by Dunnett's test (H and I).

See also Figure 2_figure supplement 1 and 2.

Figure 3. Free amino acids are transferred from skeletal muscle to BAT and the liver for maintenance of energy homeostasis

(A and B) Metabolomics analysis of amino acid concentrations in soleus and EDL muscles (A) as well as in serum and the liver (B) of control mice and mice subjected to bilateral cast immobilization for the indicated times. Results are presented as heat maps of the $\log_{10}$ value of fold change for cast-immobilized mice relative to control mice and are means of three mice per group.

(C) Organ-specific [^{3}H]leucine uptake in control mice and mice subjected to bilateral cast immobilization for 24 h (n = 4–6 per group). sWAT, subcutaneous

WAT.
(D) RT and real-time PCR analysis of SLC25A44 gene expression in sham-operated or denervated iBAT of control mice and mice subjected to subsequent bilateral cast immobilization for 24 h (n = 6 per group).
Data in (D) and (E) are means ± SEM. *p < 0.05, **p < 0.01 as determined by the unpaired t test (C) or by one-way ANOVA followed by Tukey's post hoc test (D).
See also Figure 3_figure supplement 1and 2.

Figure 4. Cast immobilization upregulates *Il6* expression in BAT and skeletal muscle
(A and B) RT and real-time PCR analysis of IL-1β, IL-6, IL-10, IL-15, TNF-α, MCP-1, BMP8B, FGF21, and irisin gene expression in iBAT (A) or soleus (B) of control mice or mice at 10 h (iBAT) or 24 h (soleus) after bilateral cast immobilization (n = 5 or 6 per group).
(C and D) RT and real-time PCR analysis of *Il6* expression in iBAT (C) and soleus (D) of control mice and mice at the indicated times after bilateral cast immobilization (n = 3–7 per group).
(E–L) RT and real-time PCR analysis of *Saa3* (E, G, I, and K) and *Socs3* (F, H, J, and L) mRNA abundance in iBAT (E and F), soleus (G and H), liver (I and J), and eWAT (K and L) of control mice and mice at the indicated times after bilateral cast immobilization (n = 3–7 per group)
(M) RT and real-time PCR analysis of *Il6* expression, respectively, in denervated iBAT of control mice or mice at the indicated times after bilateral cast immobilization (n = 4-7 per group).
(N) Serum IL-6 concentration in control mice or mice at the indicated times after bilateral cast immobilization (n = 6 per group).
All data are means ± SEM. *p < 0.05, **p < 0.01, NS (not significant) as determined by the unpaired t test (A and B) or by Dunnett's test (C–N).
See also Figure 4_figure supplement 1.

Figure 5. IL-6 affects energy metabolism in BAT and skeletal muscle of cast-immobilized mice
(A) Change in rectal body temperature during cold exposure at 4°C for 4 h for WT (n = 4 or 5) and IL-6 KO (n = 4 or 5) mice that had been subjected (or not) to bilateral cast immobilization for 24 h.

(B and C) Concentrations of carbohydrate metabolites (B) and amino acids (C) in iBAT of IL-6 KO (–/–) and WT (+/+) mice without (control) or with bilateral cast immobilization for the indicated times. Results are presented as heat maps of the $\log_{10}$ value of the fold change relative to control WT mice and are means of four mice in each group.
(D–F) RT and real-time PCR analysis of the expression of SLC25A44 (D), BCKDHA (E), and CD36 (F) genes in iBAT of IL-6 KO and WT mice without (control) or with bilateral cast immobilization for 24 h (n = 5 or 6).
(G) Incorporation of [^{3}H]leucine in iBAT of IL-6 KO and WT mice without (control) or with bilateral cast immobilization for 24 h (n = 4 or 5 per group).
(H–J) BCAA (Val, Ile, and Leu, respectively) concentrations in soleus of IL-6 KO and WT mice without (control) or with bilateral cast immobilization for 1 or 7 days (n = 4 per group).
Data in (A) and (D) through (J) are means ± SEM. *$p < 0.05$, **$p < 0.01$ as determined by one-way ANOVA followed by Tukey's post hoc test (D–G), by Dunnett's test (H–J), or by two-way ANOVA followed by Tukey's post hoc test (A).
See also Figure 5_figure supplement 1.

Figure 6. Skeletal-muscle-derived IL-6 increases BCAA concentrations in skeletal muscle for support of BAT thermogenesis
(A–C) Concentrations of BCAAs (Val, Ile, and Leu, respectively) in the soleus of control IL-6 KO mice and at 3 h after intraperitoneal administration of recombinant IL-6 (rIL-6, 400 ng) or vehicle in IL-6 KO mice that had been subjected to bilateral cast immobilization for 24 h (n = 4 or 5 per group).
(D) BCAA concentrations in C2C12 myotubes incubated in the absence or presence of rIL-6 (50 ng/ml) for 1 h (n = 6 independent experiments) .
(E) Rectal core body temperature during cold exposure at 4°C for 1 h for control IL-6 KO mice and for IL-6 KO mice subjected to bilateral cast immobilization for 24 h and injected intraperitoneally with rIL-6 (400 ng) or vehicle 30 min before cold challenge (n = 5 per group). The white circles represent control mice, the red circles indicate cast-immobilized mice, and the red triangles represent cast-immobilized mice that were treated with recombinant IL-6 (rIL-6).
(F) Rectal core body temperature during cold exposure at 4°C for 1 h for C57BL/6J mice with denervated iBAT subjected or not to bilateral cast immobilization and treatment with rIL-6 or vehicle as in (E) (n = 4 per group).

(G) Serum IL-6 concentration of mice subjected to surgical removal of iBAT and then subjected (or not, control) to bilateral cast immobilization for the indicated times (n = 4-6 per group). The white circles represent control mice, the blue circles indicate C57BL/6J mice with denervated iBAT, and the blue triangles denote C57BL/6J mice with denervated iBAT that were treated with recombinant IL-6 (rIL-6).
(H) Weight of eWAT in mice subjected to surgical removal of iBAT (or to sham surgery) followed (or not, control) by bilateral cast immobilization for 7 days (n = 5-7 per group).
(I–K) Concentrations of BCAAs (Val, Ile, and Leu, respectively) in soleus of mice subjected to surgical removal of iBAT and then subjected (or not, control) to bilateral cast immobilization for the indicated times (n = 4 per group).
All data are means ± SEM. *p < 0.05, **p < 0.01, NS (not significant) as determined by Dunnett's test (A–C and G and I-K), or by the unpaired t test (D) or by one-way ANOVA followed by Tukey's post hoc test (H), or by two-way ANOVA followed by the post hoc paired/unpaired t test with Bonferroni's correction (E and F).
See also Figure 6_figure supplement 1 and 2.

Figure 7. Acute cold exposure or restraint stress also induced IL-6 from skeletal muscle to supply BCAA for BAT thermogenesis
(A) RT and real-time PCR analysis of *Il6* expression in iBAT, soleus, liver, eWAT, and spleen of mice subjected (or not) to cold (4°C) exposure for 4 h (control, n = 6–9; cold exposure, n = 5 or 6).
(B–D) Concentrations of BCAAs (Val, Ile, and Leu, respectively) in soleus of WT and IL-6 KO mice subjected (or not) to cold exposure at 4°C for 4 h (n = 4 per group).
(E and F) RT and real-time PCR analysis of *Il6* expression in iBAT (E) and soleus (F) of control mice and mice subjected to restraint stress for 6 h (n = 4 per group).
(G–I) Concentrations of BCAAs (Val, Ile, and Leu, respectively) in soleus of WT and IL-6 KO mice subjected (or not) to restraint stress for 6 h (n = 4 per group).
All data are means ± SEM. *p < 0.05, **p < 0.01, NS (not significant) as determined by the unpaired t test (A–I).
See also Figure 7_figure supplement 1 and 2.

Supplementary Figure Legends

Figure 1_figure supplement 1.

(A–C) Weight of individual soleus (A), gastrocnemius (B), and extensor digitorum longus (EDL) muscles of control mice and mice subjected to bilateral cast immobilization of hind limbs for the indicated times (n = 5-7 per group).

(D and E) Locomotor activity during light (D) and dark (E) phases for control mice and mice subjected to bilateral cast immobilization for the indicated times (n = 6 per group).

(F) Rectal core body temperature of cast-immobilized (n = 6) and control (n = 4) mice at room temperature after bilateral cast immobilization.

(G) RT and real-time PCR analysis of the expression of UCP1 genes in iBAT of control and cast-immobilized mice subjected (or not) to cold exposure at 4°C for 4 h (n = 4-9 per group).

(H-K) RT and real-time PCR analysis of *Ucp2*, *Ucp3*, *Sln* and *Ppagc1a* expression in iBAT of control and cast-immobilized mice subjected (or not) to cold exposure at 4°C for 4 h (n = 4-9 per group).

(L) Locomotor activity during cold (4°C) exposure for 4 h determined for control mice and mice subjected to unilateral (UL) or bilateral (BL) cast immobilization (n = 5 per group). These data were obtained in conjunction with those in Figure1C.

All quantitative data are means ± SEM. *$p < 0.05$, **$p < 0.01$, NS (not significant) as determined by Dunnett's test (A-C) or by two-way ANOVA followed by Tukey's post hoc test or the post hoc paired/unpaired t test with Bonferroni's correction (D-F and L), or by the unpaired t test (G-K)

Figure 1_figure supplement 2.

(A) Concentrations of carbohydrate metabolites (acetyl CoA divalent, succinic acid, fumaric acid and malic acid) in soleus and EDL of control mice and mice subjected to bilateral cast immobilization for the indicated times. Results are presented as heat maps of the $\log_{10}$ value of fold change for cast-immobilized mice relative to control mice and are are shown individually for three mice of each group.

(B and C) RT and real-time PCR analysis of *Ucp3* and *Ucp2* expression, respectively, in soleus of control mice and mice subjected to bilateral cast immobilization for the indicated times (n = 5-6 per group).

(D and E) RT and real-time PCR analysis of *Sln* and *Camk2a* expression,

respectively, in soleus of control mice and mice subjected to bilateral cast immobilization for the indicated times (n = 6 per group).
(F and G) RT and real-time PCR analysis of *Ppargc1a*, and *Tfam* expression, respectively, in soleus of control mice and mice subjected to bilateral cast immobilization for the indicated times (n = 6 per group).
(H) Hematoxylin-eosin staining of surgically denervated or sham-operated iBAT from control mice or mice subjected to bilateral cast immobilization for 7 days. Scale bar, 50 µm.
(I) Food intake of control mice and mice subjected to bilateral cast immobilization for the indicated times (n = 6–9 per group).
(J) Hematoxylin-eosin staining of iBAT of control mice and mice subjected to bilateral cast immobilization for 1 or 7 days. Scale bar, 50 µm.
All quantitative data other than those in (A, H and J) are means ± SEM. *p < 0.05, **p < 0.01, NS (not significant) as determined by Dunnett's test (B-G) or by two-way ANOVA followed by Tukey's post hoc test or the post hoc paired/unpaired t test with Bonferroni's correction (I).

Figure 2_figure supplement 1.
(A) Pathway analysis of metabolites upregulated in iBAT by cast immobilization for 10 h.
(B and C) Oxygen consumption rate (VO_2) and RER, respectively, for mice with denervated iBAT subjected (or not) to bilateral cast immobilization for 7 days (n = 3 per group).
Quantitative data other than in (A) are means ± SEM. *p < 0.05, **p < 0.01, as determined by two-way ANOVA followed by Tukey's post hoc test or the post hoc paired/unpaired t test with Bonferroni's correction (B and C).

Figure 2_figure supplement 2.
(A and B) RT and real-time PCR analysis of G6Pase (*G6pc1*) and PEPCK (*Pck1*) gene expression in the liver of control mice and mice subjected to bilateral cast immobilization for the indicated times (n = 5 or 6 per group).
(C) Concentrations of carbohydrate metabolites in the liver of control mice and mice subjected to bilateral cast immobilization for the indicated times. The metabolomics data are presented as heat maps corresponding to the $\log_{10}$ value of fold change in cast-immobilized mice relative to control mice. Results are means of three mice per group.

(D) Serum concentration of noradrenaline in control mice and mice subjected to bilateral cast immobilization for the indicated times (n = 5–7 per group).
(E) Serum concentration of corticosterone for control mice and mice subjected to bilateral cast immobilization for the indicated times (n = 6–8 per group).
(F) RT and real-time PCR analysis of *Crh* expression in the hypothalamus of control mice and mice subjected to bilateral cast immobilization for the indicated times (n = 5–8 per group).
Quantitative data other than in (C) are means ± SEM. *p < 0.05, **p < 0.01, NS (not significant) as determined by Dunnett's test (A, B and D-F).

Figure 3_figure supplement 1.
(A and B) RT and real-time PCR analysis of *Fbxo32* (Atrogin-1) and *Trim63* (MuRF-1) expression in the soleus muscle of control mice and mice subjected to bilateral cast immobilization for the indicated times (n = 6 per group).
(C–H) RT and real-time PCR analysis of SLC1A5, SLC7A5, SLC38A2, SLC43A1, BCAT2, and BCKHDA gene expression, respectively, in iBAT of control mice or mice subjected to bilateral cast immobilization for the indicated times (n = 3–6 per group).
(I–M) RT and real-time PCR analysis of gene expression for SLC1A5, SLC7A5, SLC38A2, SLC43A1, and BCKHDA, respectively, in the liver of control mice or mice subjected to bilateral cast immobilization for the indicated times (n = 6 per group).
(N–S) RT and real-time PCR analysis of gene expression for SLC1A5, SLC7A5, SLC38A2, SLC43A1, BCAT2, and BCKHDA in soleus of control mice or mice subjected to bilateral cast immobilization for the indicated times (n = 6 per group).
All data are means ± SEM. *p < 0.05, **p < 0.01 as determined by Dunnett's test.

Figure 3_figure supplement 2.
(A–C) RT and real-time PCR analysis of SLC25A44 gene expression in iBAT (A), liver (B), and soleus (C) of control mice or mice subjected to bilateral cast immobilization for the indicated times (n = 6 per group).
(D–J) RT and real-time PCR analysis of gene expression for SLC25A44, SLC1A5, SLC7A5, SLC38A2, SLC43A1, BCAT2, and BCKDHA, respectively, in denervated iBAT of control mice or mice subjected to bilateral cast

immobilization for the indicated times (n = 4–6 per group).
All data are means ± SEM. *p < 0.05, **p < 0.01 as determined by Dunnett's test.

Figure 4_figure supplement 1.
(A–G) RT and real-time PCR analysis of TNF-α, MCP-1, IL-1β, IL-10, IL-15, FGF21, and BMP8B gene expression, respectively, in iBAT of control mice and mice at the indicated times after bilateral cast immobilization (n = 3–6 per group).
(H–N) RT and real-time PCR analysis of TNF-α, MCP-1, IL-1β, IL-10, IL-15, FGF21, and irisin gene expression, respectively, in soleus of control mice and mice at the indicated times after bilateral cast immobilization (n = 5 or 6 per group).
(O–Q) RT and real-time PCR analysis of *Il6* expression in liver (O), eWAT (P), and spleen (Q) of control mice and mice at the indicated times after bilateral cast immobilization (n = 5-6 per group).
(R) Serum concentration of TNF-α in control mice and mice at the indicated times after bilateral cast immobilization (n = 6 per group).
All data are means ± SEM. *p < 0.05, **p < 0.01, NS (not significant) as determined by Dunnett's test.

Figure 5_figure supplement 1.
(A) RT and real-time PCR analysis of *Ucp1* mRNA abundance in iBAT of WT and IL-6 KO mice without (control) or with bilateral cast immobilization for 1 or 7 days (n = 5 or 6 per group).
(B and C) Oxygen consumption rate for WT (B) and IL-6 KO (C) mice subjected (or not) to bilateral cast immobilization for 7 days (n = 4 per group).
(D) Hematoxylin-eosin staining of iBAT from IL-6 KO and WT mice without (control) or with bilateral cast immobilization for 7 days. Scale bar, 50 µm.
(E and F) RER for WT (E) and IL-6 KO (F) mice subjected (or not) to bilateral cast immobilization for 7 days (n = 4 per group).
(G) Weight of eWAT in WT (+/+) and IL-6 KO (-/- mice subjected (or not, control) to bilateral cast immobilization for 7 days (n = 5-7 per group).
(H–J) Serum concentrations of BCAA (Val, Ile, and Leu, respectively) concentrations of IL-6 KO and WT mice without (control) or with bilateral cast immobilization for 1 or 7 days (n = 4 per group).

All data other than those in (F) are means ± SEM. *p < 0.05, **p < 0.01 as determined by one-way ANOVA followed by Tukey's post hoc test (A and G) or by two-way ANOVA followed by Tukey's post hoc test or the post hoc paired/unpaired t test with Bonferroni's correction (B-C and E-F), or by Dunnett's test (H-I).

Figure 6_figure supplement 1.

(A) Amino acid concentrations in soleus of control IL-6 KO mice and at 3 h after intraperitoneal administration of recombinant IL-6 (rIL-6, 400 ng) or vehicle in IL-6 KO mice that had been subjected to bilateral cast immobilization for 24 h. Results are presented as heat maps of the $\log_{10}$ value of the fold change relative to control mice and are means of four or five mice in each group.

(B and C) RT and real-time PCR analysis of *Saa3* (B) and *Socs3* (C) mRNA abundance in C2C12 myotubes incubated in the absence or presence of rIL-6 (50 ng/ml) for 1 h (n = 8 or 9 independent experiments).

(D) Amounts of carbohydrate metabolites in iBAT of mice as in (A). Results are presented as heat maps of the $\log_{10}$ value of the fold change relative to control mice and are means of four mice in each group.

(E) Amino acid concentrations in iBAT of mice as in (A). Results are presented as heat maps of the $\log_{10}$ value of the fold change relative to control mice and are means of four or five mice in each group.

(F–H) RT and real-time PCR analysis of UCP1 (F), SLC25A44 (G), and BCKDHA (H) gene expression in iBAT of mice as in (A) (n = 5 per group).

(I) Change in rectal core body temperature of mice of the indicated *Il6* genotypes during cold exposure at 4°C for 4 h (+/+ and –/–, n = 5; +/–, n = 6).

(J) RT and real-time PCR analysis of *Ucp1* mRNA abundance in iBAT of mice of the indicated *Il6* genotypes (n = 5 or 6 per group).

(K–M) RT and real-time PCR analysis of UCP1 (K), SLC25A44 (L), and BCKDHA (M) gene expression in cultured brown adipocytes incubated in the absence or presence of rIL-6 (50 ng/ml) or CL316 243 (1 µM) for 24 h (n = 3 or 4 independent experiments).

(N–P) RT and real-time PCR analysis of UCP1 (N), SLC25A44 (O) and BCKDHA (P) gene expression in iBAT of WT (+/+, n = 5 per group) or IL-6 KO (–/–, n = 8 per group) mice after intraperitoneal treatment with CL316 243 (0.1 mg/kg per day) or vehicle for 7 days.

All data other than those in (A),(D) and (E) are means ± SEM. *p < 0.05, **p <

0.01, ***p < 0.001 as determined by the unpaired t test (B and C), by one-way ANOVA followed by Tukey's post hoc test (F–H and J-P), or by two-way ANOVA followed by the post hoc paired/unpaired t test with Bonferroni's correction (I).

Figure 6_figure supplement 2.
(A-E) RT and real-time PCR analysis of SLC43A1, SLC1A5, SLC7A5, BCAT2, and BCKDHA gene expression, respectively, in soleus of iBAT-depleted mice subjected (or not, control) to bilateral cast immobilization for the indicated times (n = 4–7 per group).
(F) Change in soleus and gastrocnemius muscle weights of iBAT-depleted or sham-operated mice subjected to bilateral cast immobilization for 7 days (n = 6 per group).
All data are means ± SEM. *p < 0.05, **p < 0.01, ***p < 0.001 as determined by the unpaired t test (F) or by Dunnett's test (A-E).
See also Tables S2.

Figure 7_figure supplement 1.
(A-E) RT and real-time PCR analysis of *Il6*, *Saa3*, *Socs3*, *Fbxo32* and *Trim63* mRNA abundance in BBM of mice subjected (or not, control) to bilateral cast immobilization for the indicated times (n = 4 per group).
(F-H) BCAA (Val, Ile, and Leu, respectively) concentrations in BBM of mice subjected (or not, control) to bilateral cast immobilization for the indicated times (n = 4 per group).
(I and J) RT and real-time PCR analysis of *Saa3* (I) and *Socs3* (J) mRNA abundance in soleus of mice subjected (or not) to cold (4°C) exposure for 4 h (control, n = 6; cold exposure, n = 5).
(K and L) RT and real-time PCR analysis of *Fbox32* (K) and *Trim63* (L) mRNA abundance in soleus of mice subjected (or not) to cold (4°C) exposure for 4 h (control, n = 6; cold exposure, n = 5).
(M and N) Weight of individual soleus (M) and gastrocnemius (N) muscles of control mice and mice subjected to. cold exposure at 4°C for 4 h (n = 5 or 6 per group).
(O) Amino acid concentrations in soleus of WT (+/+) and IL-6 KO (–/–) mice subjected (or not) to cold exposure at 4°C for 4 h. Results are presented as heat maps of the $\log_{10}$ value of fold change relative to WT control mice and are means of four mice in each group.

(P) BCAA concentrations in soleus of iBAT-depleted mice subjected (or not, control) to cold exposure at 4°C for 4 h (n = 3 or 4 per group).
All data other than in (O) are means ± SEM. *p < 0.05, **p < 0.01, ***p < 0.001 as determined by the unpaired t test (I-N and P) or by Dunnett's test (A-H).

Figure 7_figure supplement 2.
(A) RT and real-time PCR analysis of *Ucp1* mRNA abundance in iBAT of mice subjected (or not) to restraint stress for 6 h (n = 4 per group).
(B and C) RT and real-time PCR analysis of *Saa3* (B) and *Socs3* (C) mRNA abundance in soleus of mice subjected (or not) to restraint stress for 6 h (n = 4 per group).
(D-F) Weight of soleus (D), gastrocnemius (E) and EDL (F) in mice subjected to restraint stress for 6 h (n = 4 per group).
(G and H) RT and real-time PCR analysis of *Fbox32* (G) and *Trim63* (H) mRNA abundance in soleus of mice subjected (or not) to restraint stress for 6 h (n = 4 per group).
(I) Amino acid concentrations in soleus of WT (+/+) and IL-6 KO (–/–) mice subjected (or not) to restraint stress for 6 h. Results are presented as heat maps of the $\log_{10}$ value of fold change relative to WT control mice and are means of four mice in each group.
All data are means ± SEM. *p < 0.05 as determined by the unpaired t test (A-H) .

Fig.1

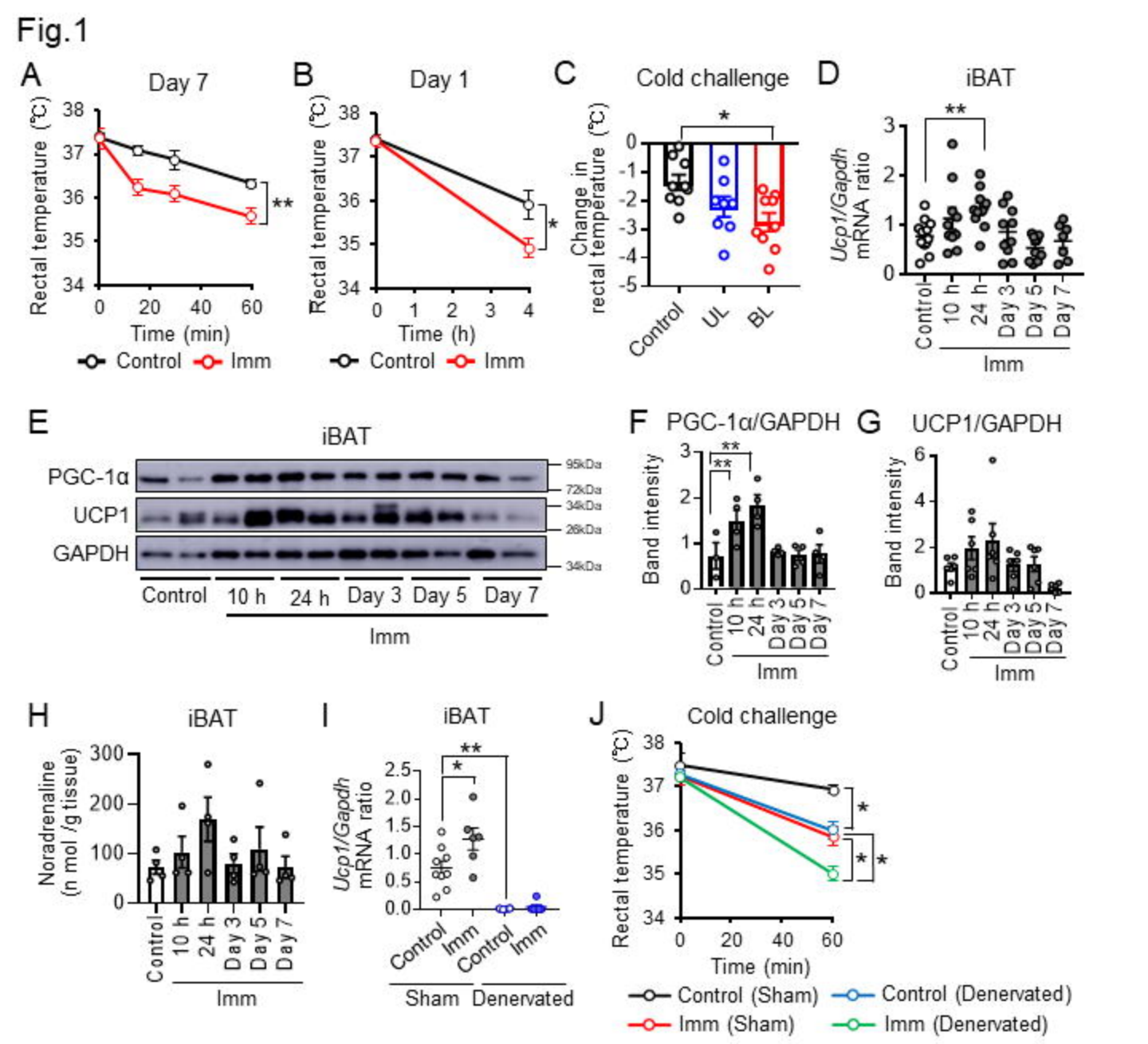
A
Day 7
Rectal temperature (℃)
Time (min)
Control
Imm
B
Day 1
Rectal temperature (℃)
Time (h)
Control
Imm
C
Cold challenge
Change in rectal temperature (℃)
Control
UL
BL
D
iBAT
Ucp1/Gapdh mRNA ratio
Control
10 h
24 h
Day 3
Day 5
Day 7
Imm
E
iBAT
PGC-1α
UCP1
GAPDH
95kDa
72kDa
34kDa
26kDa
34kDa
Control
10 h
24 h
Day 3
Day 5
Day 7
Imm
F
PGC-1α/GAPDH
Band intensity
Control
10 h
24 h
Day 3
Day 5
Day 7
Imm
G
UCP1/GAPDH
Band intensity
Control
10 h
24 h
Day 3
Day 5
Day 7
Imm
H
iBAT
Noradrenaline (n mol /g tissue)
Control
10 h
24 h
Day 3
Day 5
Day 7
Imm
I
iBAT
Ucp1/Gapdh mRNA ratio
Control
Imm
Control
Imm
Sham
Denervated
J
Cold challenge
Rectal temperature (℃)
Time (min)
Control (Sham)
Control (Denervated)
Imm (Sham)
Imm (Denervated)

Fig.2

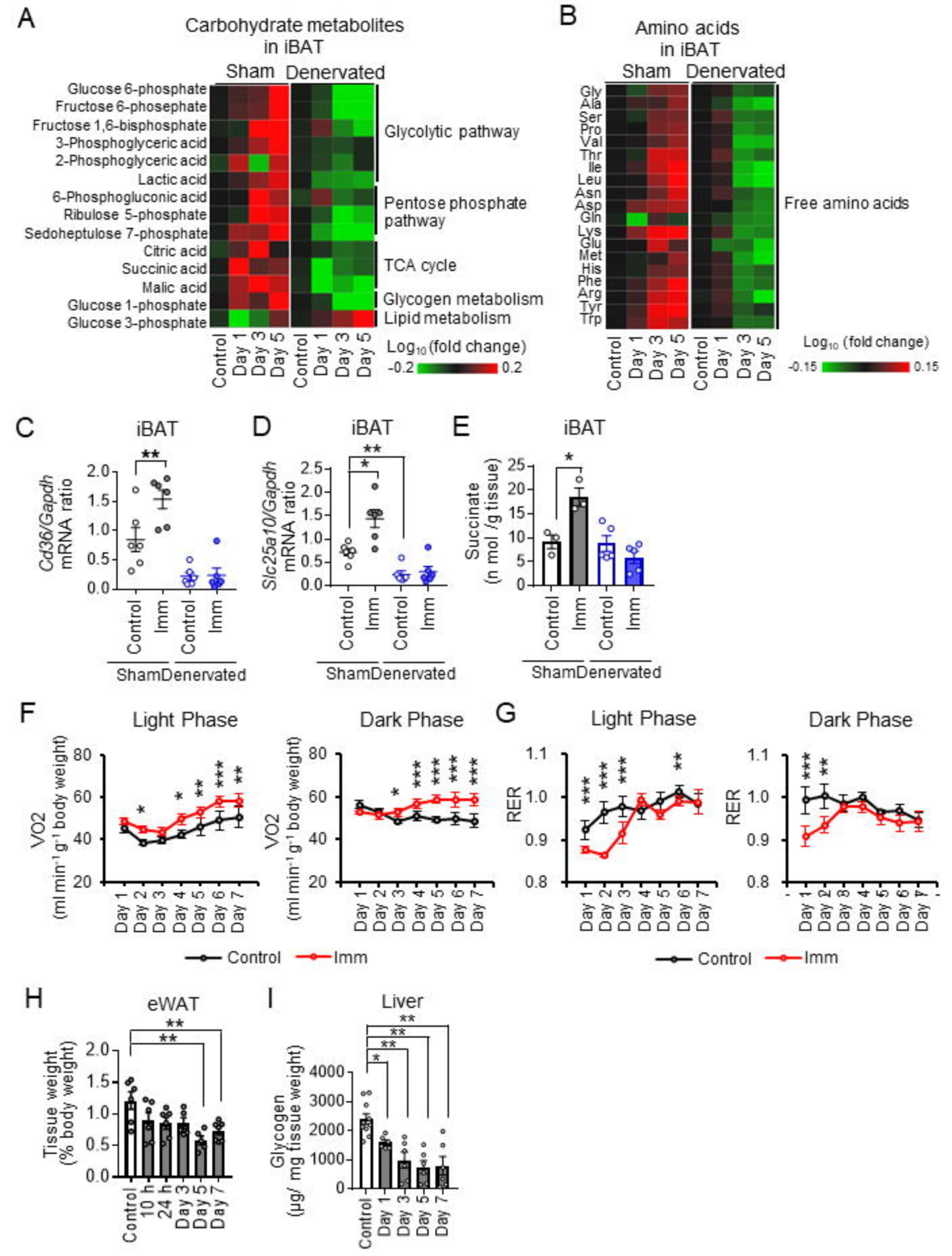
A
Carbohydrate metabolites in iBAT
Sham
Denervated
Glucose 6-phosphate
Fructose 6-phosephate
Fructose 1,6-bisphosphate
3-Phosphoglyceric acid
2-Phosphoglyceric acid
Lactic acid
6-Phosphogluconic acid
Ribulose 5-phosphate
Sedoheptulose 7-phosphate
Citric acid
Succinic acid
Malic acid
Glucose 1-phosphate
Glucose 3-phosphate
Glycolytic pathway
Pentose phosphate pathway
TCA cycle
Glycogen metabolism
Lipid metabolism
Control
Day 1
Day 3
Day 5
Log10 (fold change)
-0.2
0.2
B
Amino acids in iBAT
Gly
Ala
Ser
Pro
Val
Thr
Ile
Leu
Asn
Asp
Gln
Lys
Glu
Met
His
Phe
Arg
Tyr
Trp
Free amino acids
-0.15
0.15
C
iBAT
Cd36/Gapdh mRNA ratio
Control
Imm
ShamDenervated
D
Slc25a10/Gapdh mRNA ratio
E
Succinate (n mol /g tissue)
F
Light Phase
Dark Phase
VO2 (ml min-1 g-1 body weight)
Day 1
Day 2
Day 3
Day 4
Day 5
Day 6
Day 7
G
RER
H
eWAT
Tissue weight (% body weight)
10 h
24 h
I
Liver
Glycogen (μg/ mg tissue weight)

Fig.3

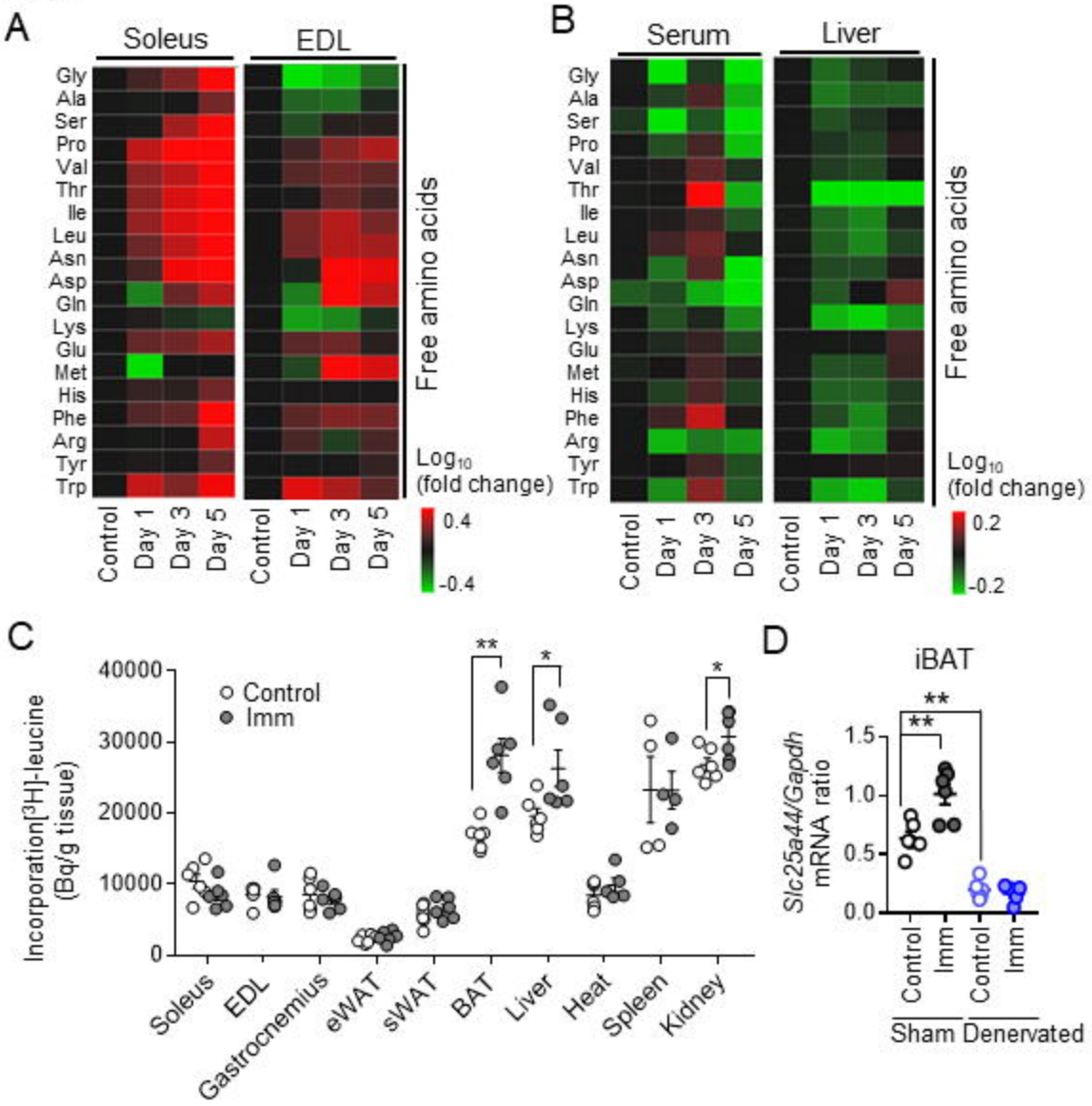
A
Soleus
EDL
Gly
Ala
Ser
Pro
Val
Thr
Ile
Leu
Asn
Asp
Gln
Lys
Glu
Met
His
Phe
Arg
Tyr
Trp
Free amino acids
Log10 (fold change)
0.4
-0.4
Control
Day 1
Day 3
Day 5
B
Serum
Liver
0.2
-0.2
C
Incorporation[3H]-leucine (Bq/g tissue)
40000
30000
20000
10000
0
Control
Imm
**
*
Soleus
EDL
Gastrocnemius
eWAT
sWAT
BAT
Liver
Heat
Spleen
Kidney
D
iBAT
Slc25a44/Gapdh mRNA ratio
1.5
1.0
0.5
0.0
Sham
Denervated

Fig.4

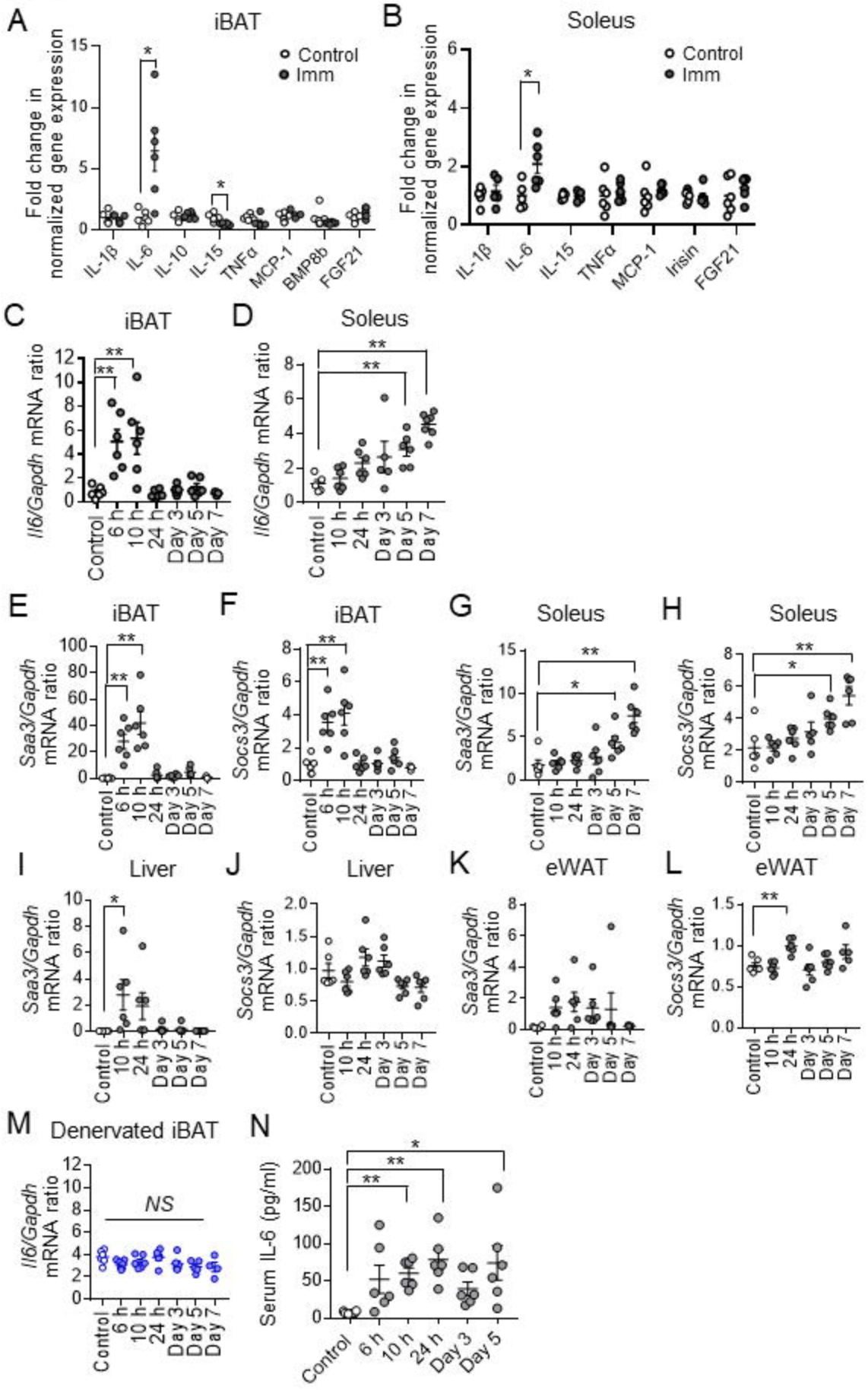
A
iBAT
Fold change in normalized gene expression
Control
Imm
IL-1β
IL-6
IL-10
IL-15
TNFα
MCP-1
BMP8b
FGF21
B
Soleus
Fold change in normalized gene expression
Control
Imm
IL-1β
IL-6
IL-15
TNFα
MCP-1
Irisin
FGF21
C
iBAT
Il6/Gapdh mRNA ratio
Control
6 h
10 h
24 h
Day 3
Day 5
Day 7
D
Soleus
Il6/Gapdh mRNA ratio
Control
10 h
24 h
Day 3
Day 5
Day 7
E
iBAT
Saa3/Gapdh mRNA ratio
F
iBAT
Socs3/Gapdh mRNA ratio
G
Soleus
Saa3/Gapdh mRNA ratio
H
Soleus
Socs3/Gapdh mRNA ratio
I
Liver
Saa3/Gapdh mRNA ratio
J
Liver
Socs3/Gapdh mRNA ratio
K
eWAT
Saa3/Gapdh mRNA ratio
L
eWAT
Socs3/Gapdh mRNA ratio
M
Denervated iBAT
Il6/Gapdh mRNA ratio
NS
N
Serum IL-6 (pg/ml)
Control
6 h
10 h
24 h
Day 3
Day 5

Fig.5

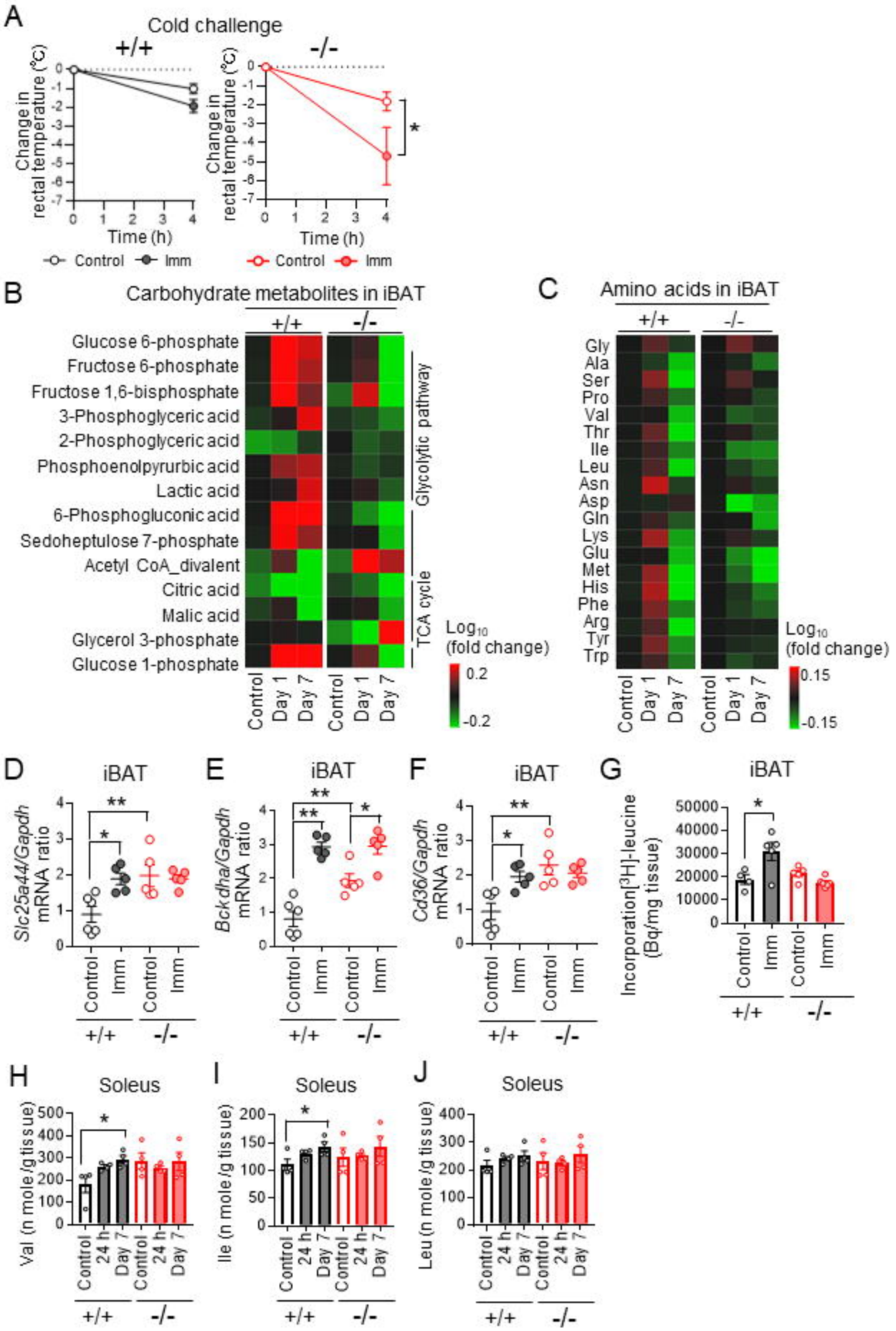
A
Cold challenge
+/+
-/-
Change in rectal temperature (°C)
Time (h)
Control
Imm
*
B
Carbohydrate metabolites in iBAT
+/+
-/-
Glucose 6-phosphate
Fructose 6-phosphate
Fructose 1,6-bisphosphate
3-Phosphoglyceric acid
2-Phosphoglyceric acid
Phosphoenolpyrurbic acid
Lactic acid
6-Phosphogluconic acid
Sedoheptulose 7-phosphate
Acetyl CoA_divalent
Citric acid
Malic acid
Glycerol 3-phosphate
Glucose 1-phosphate
Glycolytic pathway
TCA cycle
Control
Day 1
Day 7
Log10 (fold change)
0.2
-0.2
C
Amino acids in iBAT
Gly
Ala
Ser
Pro
Val
Thr
Ile
Leu
Asn
Asp
Gln
Lys
Glu
Met
His
Phe
Arg
Tyr
Trp
0.15
-0.15
D
iBAT
Slc25a44/Gapdh mRNA ratio
E
Bckdha/Gapdh mRNA ratio
F
Cd36/Gapdh mRNA ratio
G
Incorporation[3H]-leucine (Bq/mg tissue)
H
Soleus
Val (n mole/g tissue)
I
Ile (n mole/g tissue)
J
Leu (n mole/g tissue)
24 h

Fig.6

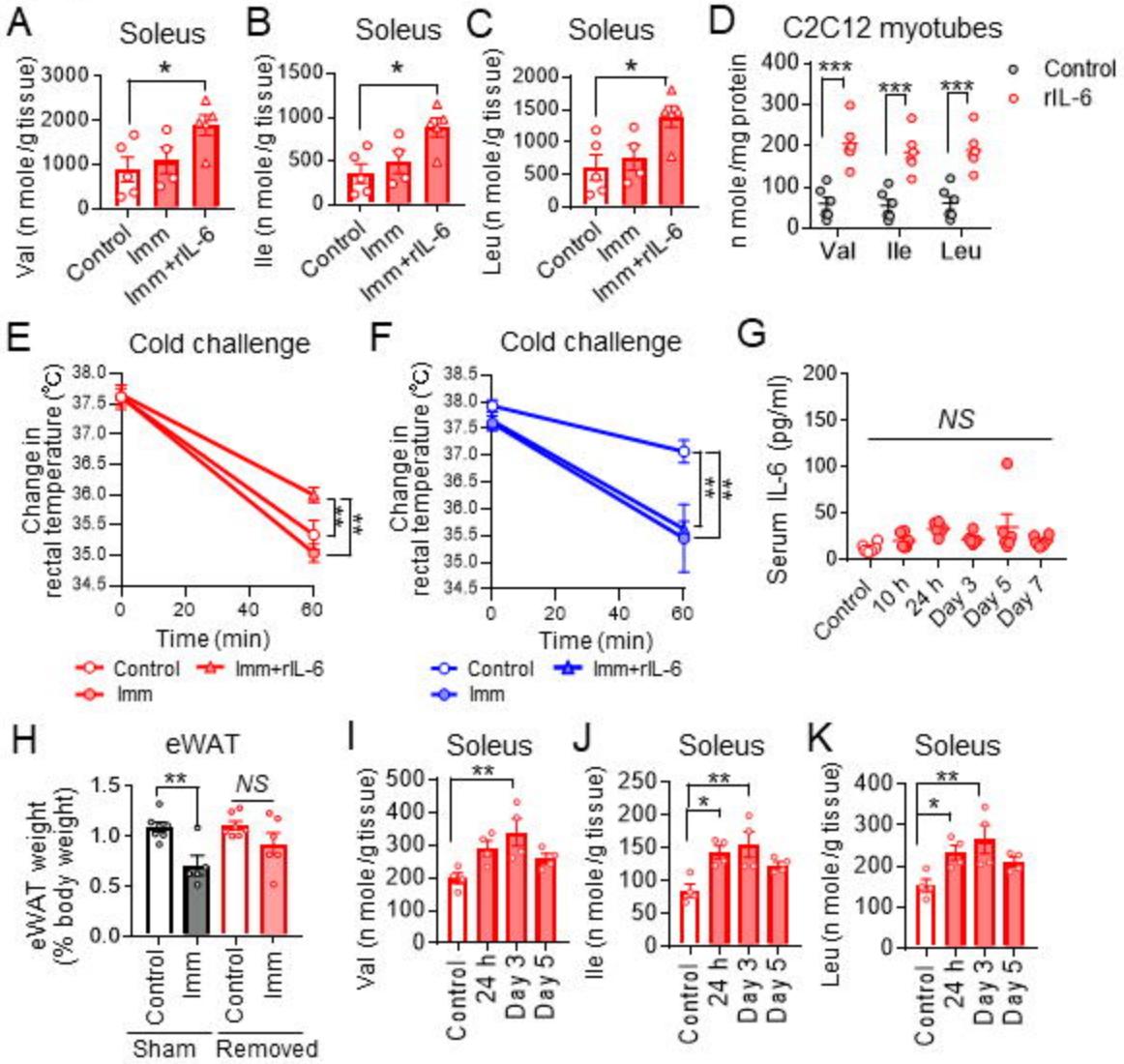
A
Soleus
Val (n mole /g tissue)
3000
2000
1000
0
*
Control
Imm
Imm+rIL-6
B
Soleus
Ile (n mole /g tissue)
1500
1000
500
0
*
Control
Imm
Imm+rIL-6
C
Soleus
Leu (n mole /g tissue)
2000
1500
1000
500
0
*
Control
Imm
Imm+rIL-6
D
C2C12 myotubes
n mole /mg protein
400
300
200
100
0
***
***
***
Control
rIL-6
Val
Ile
Leu
E
Cold challenge
Change in rectal temperature (°C)
38.0
37.5
37.0
36.5
36.0
35.5
35.0
34.5
0
20
40
60
Time (min)
**
**
Control
Imm+rIL-6
Imm
F
Cold challenge
Change in rectal temperature (°C)
38.5
38.0
37.5
37.0
36.5
36.0
35.5
35.0
34.5
0
20
40
60
Time (min)
**
**
Control
Imm+rIL-6
Imm
G
Serum IL-6 (pg/ml)
200
150
100
50
0
NS
Control
10 h
24 h
Day 3
Day 5
Day 7
H
eWAT
eWAT weight (% body weight)
1.5
1.0
0.5
0.0
**
NS
Control
Imm
Control
Imm
Sham
Removed
I
Soleus
Val (n mole /g tissue)
500
400
300
200
100
0
**
Control
24 h
Day 3
Day 5
J
Soleus
Ile (n mole /g tissue)
250
200
150
100
50
0
*
**
Control
24 h
Day 3
Day 5
K
Soleus
Leu (n mole /g tissue)
400
300
200
100
0
*
**
Control
24 h
Day 3
Day 5

Fig.7

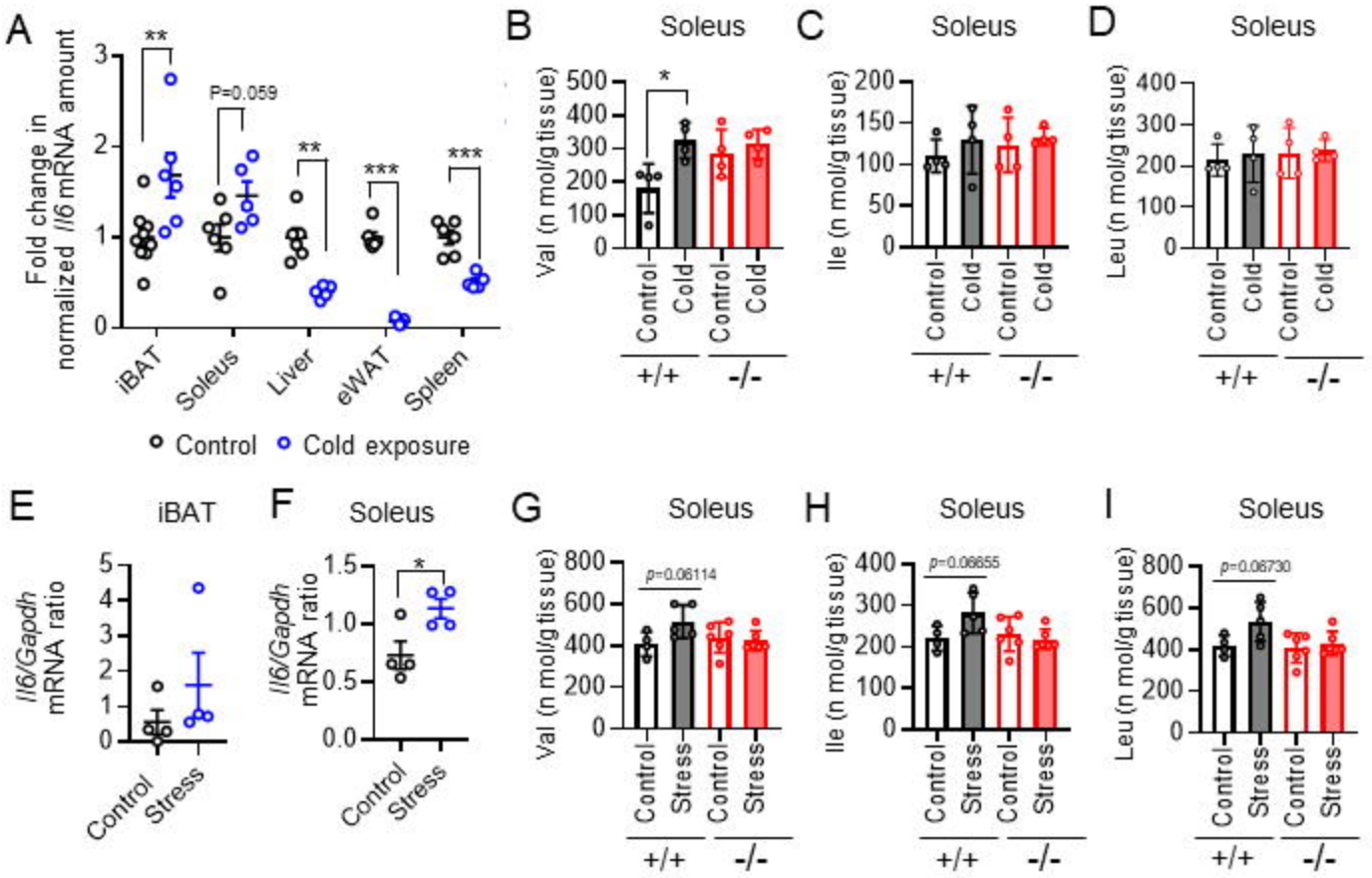
A
Fold change in normalized Il6 mRNA amount
**
P=0.059
**
***
***
iBAT
Soleus
Liver
eWAT
Spleen
Control
Cold exposure
B
Soleus
Val (n mol/g tissue)
*
Control
Cold
Control
Cold
+/+
-/-
C
Soleus
Ile (n mol/g tissue)
D
Soleus
Leu (n mol/g tissue)
E
iBAT
Il6/Gapdh mRNA ratio
Control
Stress
F
Soleus
Il6/Gapdh mRNA ratio
*
G
Soleus
Val (n mol/g tissue)
p=0.06114
Stress
H
Soleus
Ile (n mol/g tissue)
p=0.06655
I
Soleus
Leu (n mol/g tissue)
p=0.06730

Fudure1_figure supplement 1

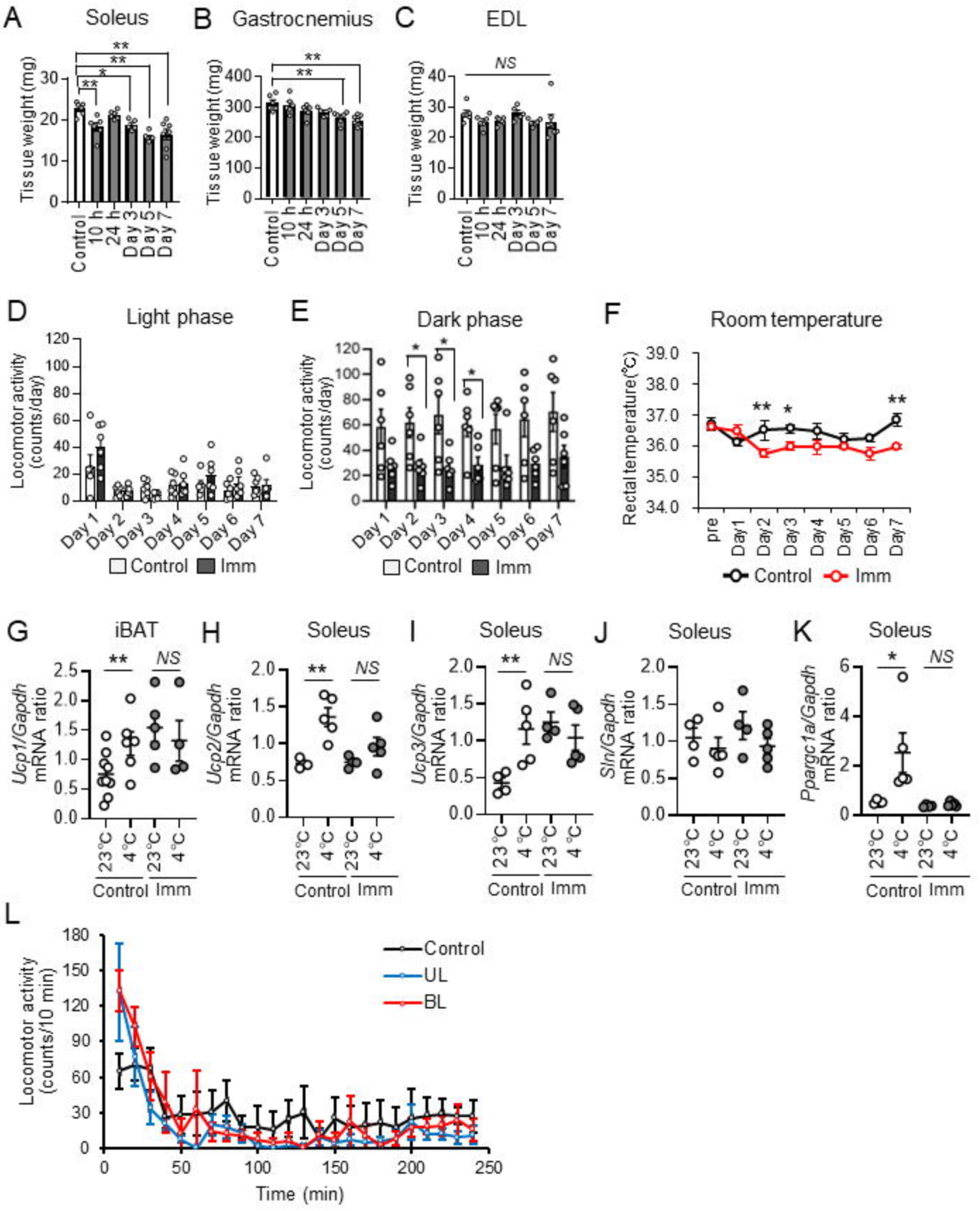

Figure 1_figure supplement 2

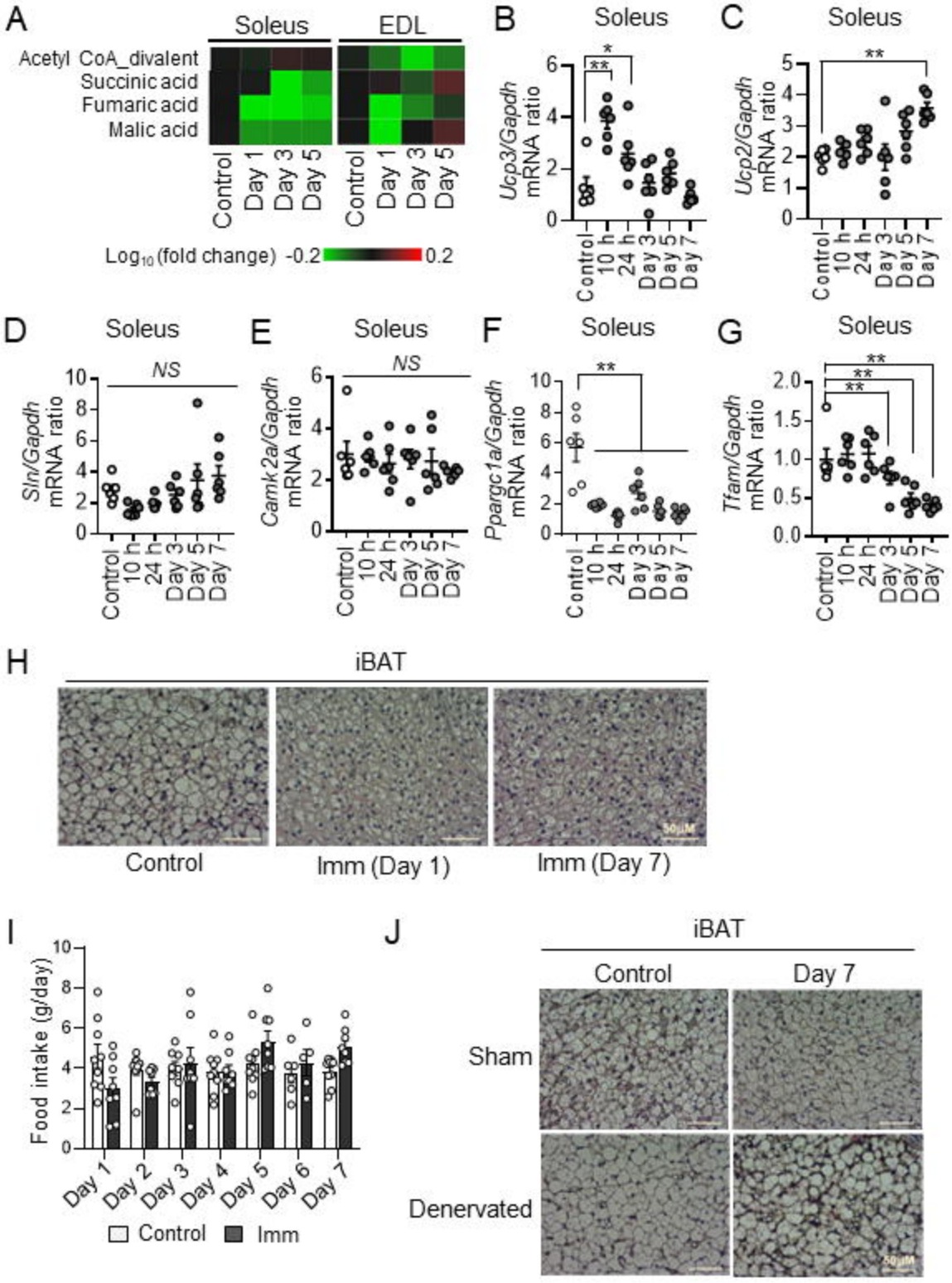

Figure 2_figure supplement 1

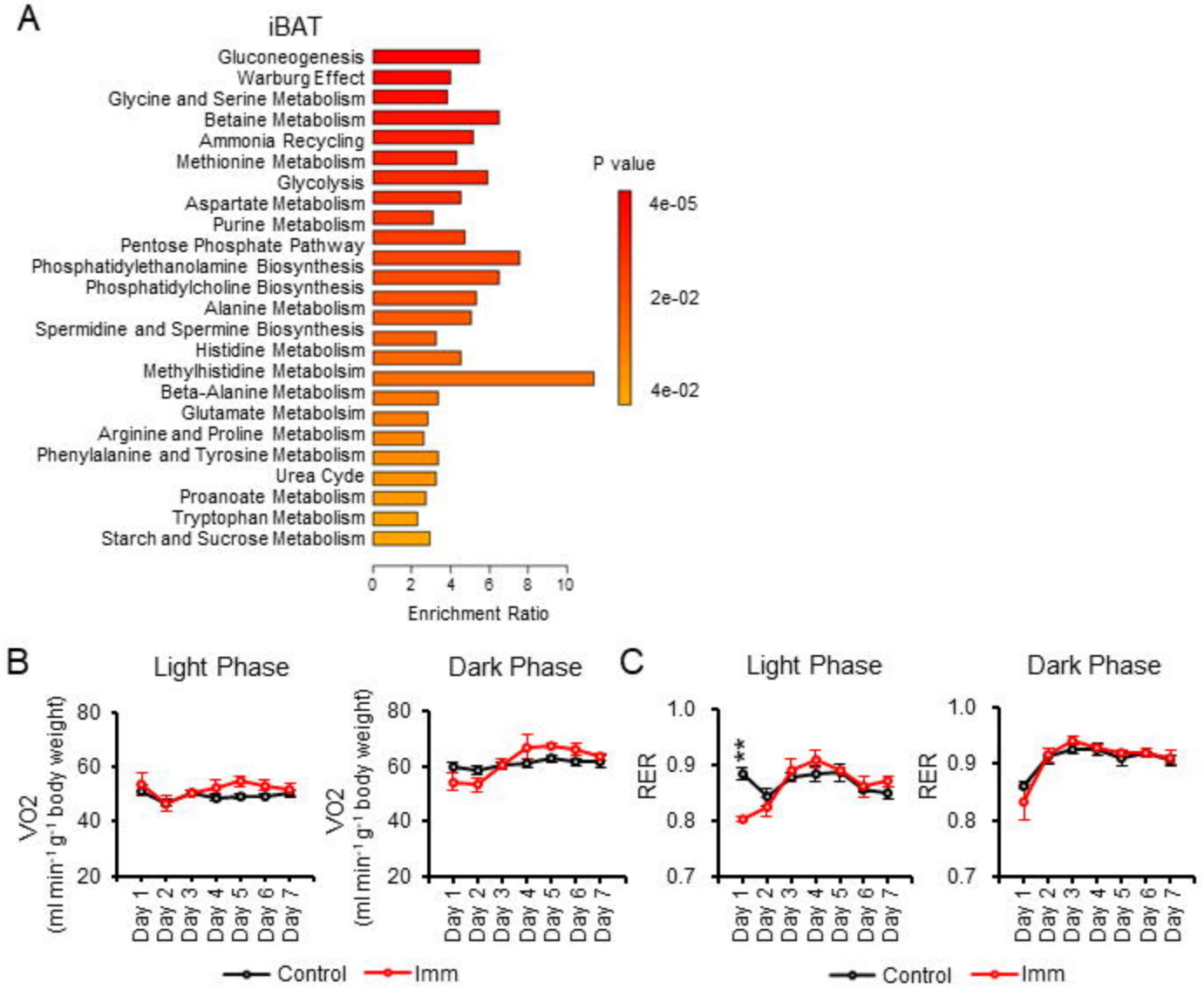

Figure 2_figure supplement 2

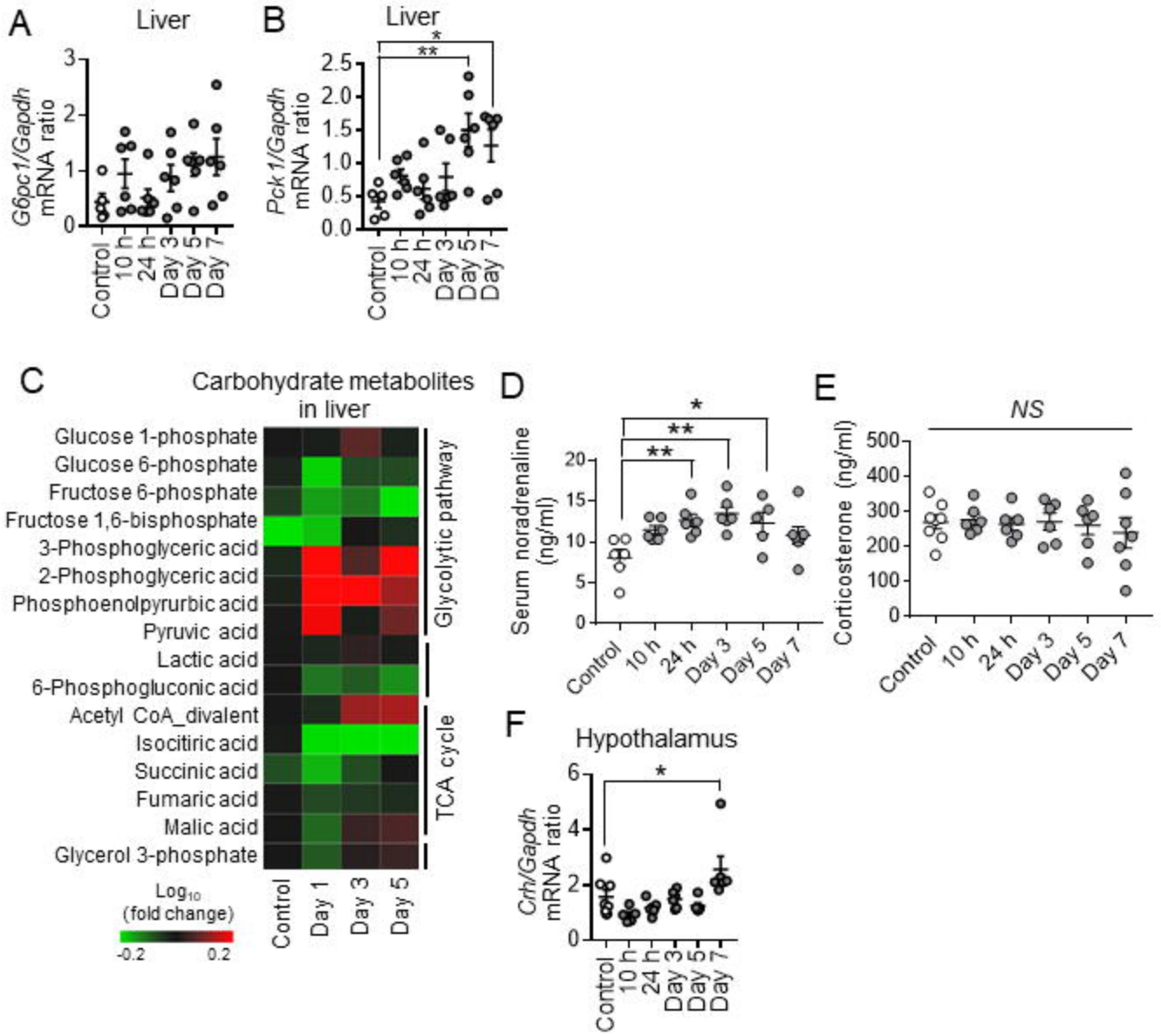

Figure 3_figure supplement 1

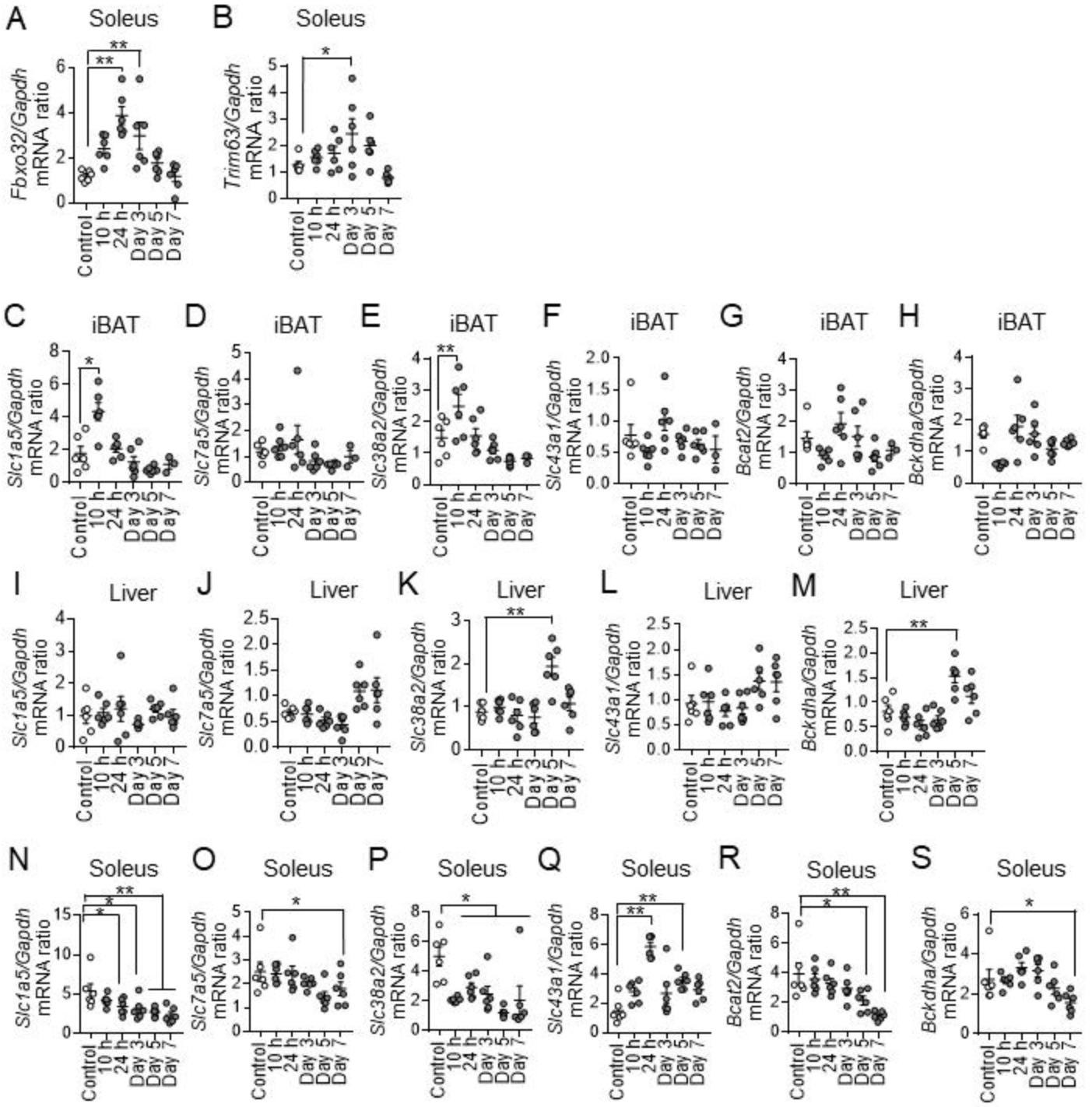

Figure 3_figure supplement 2

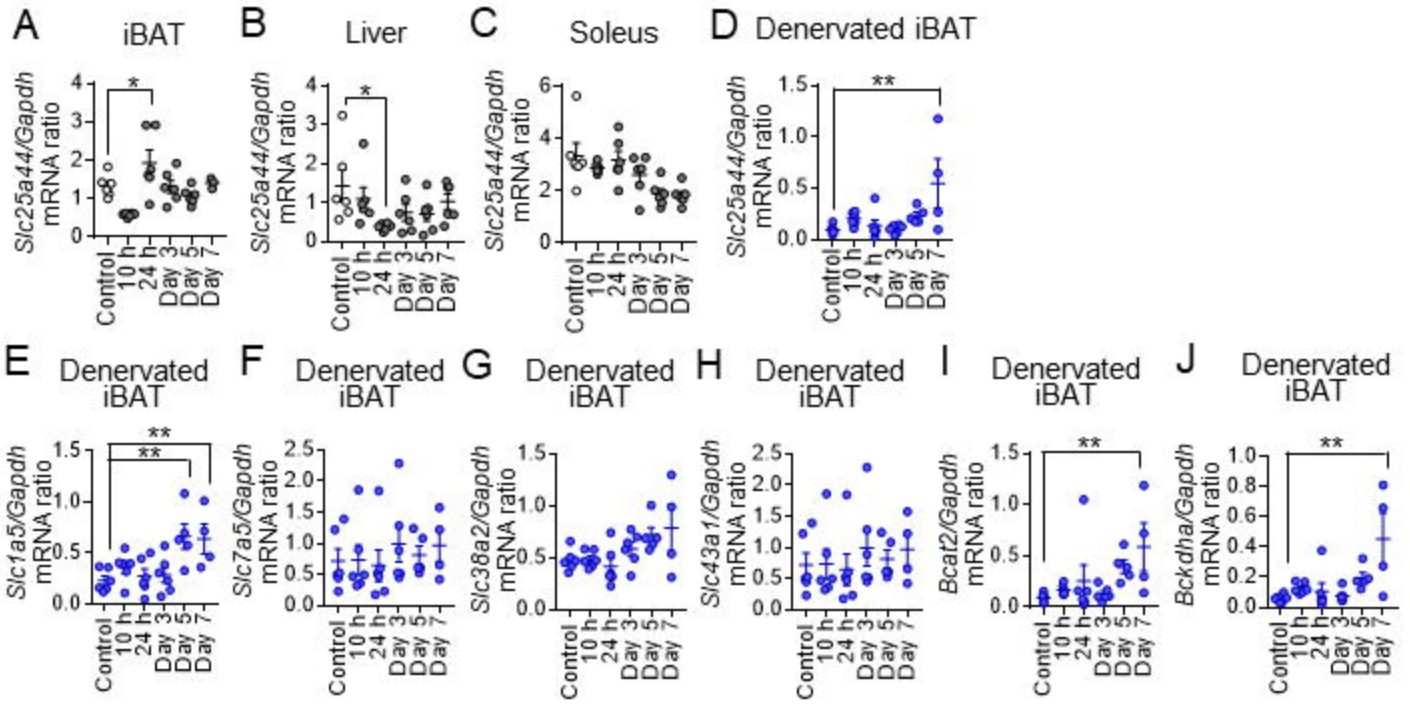

Figure 4_figure supplement 1

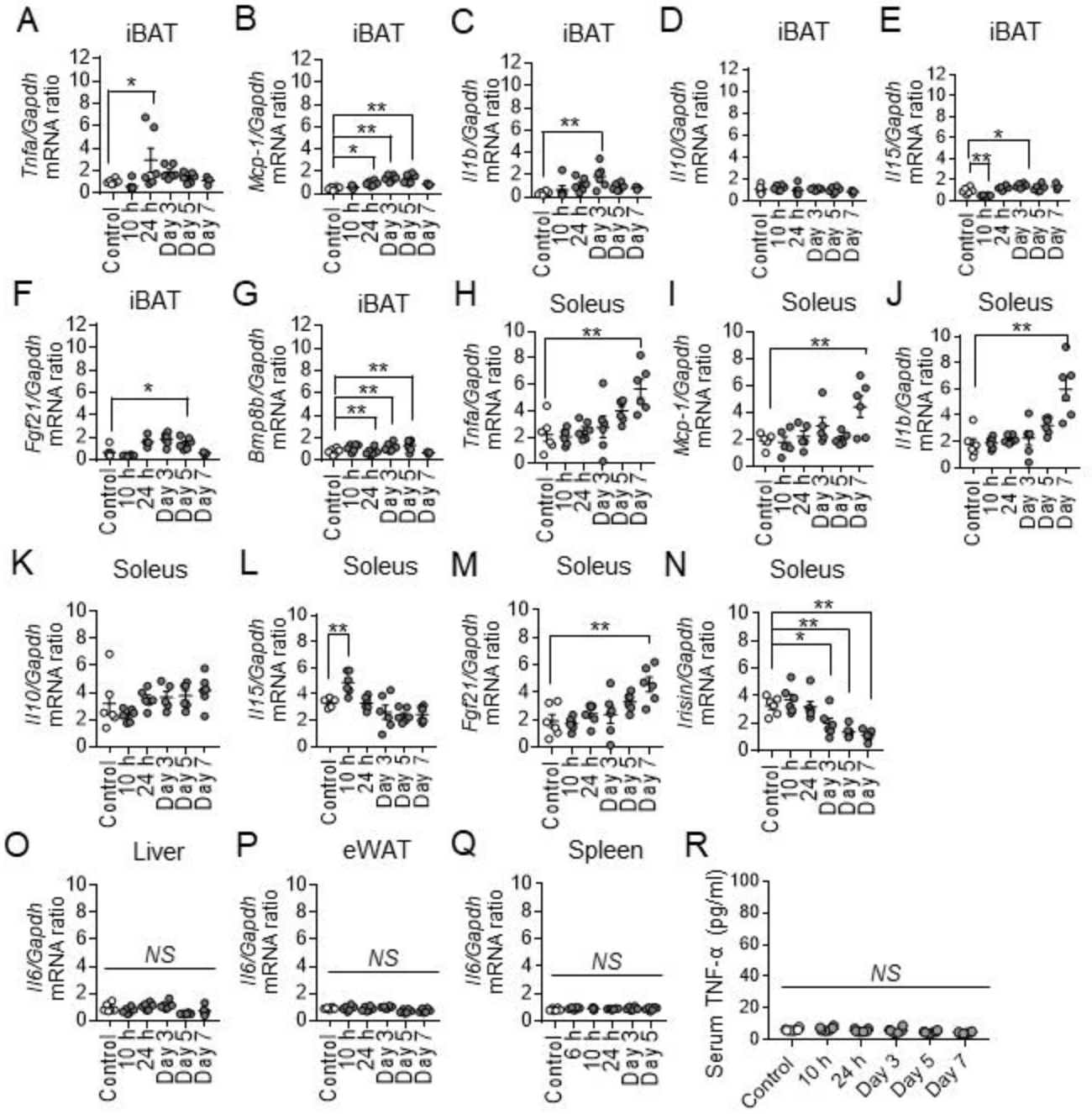

Figure 5_figure supplement 1

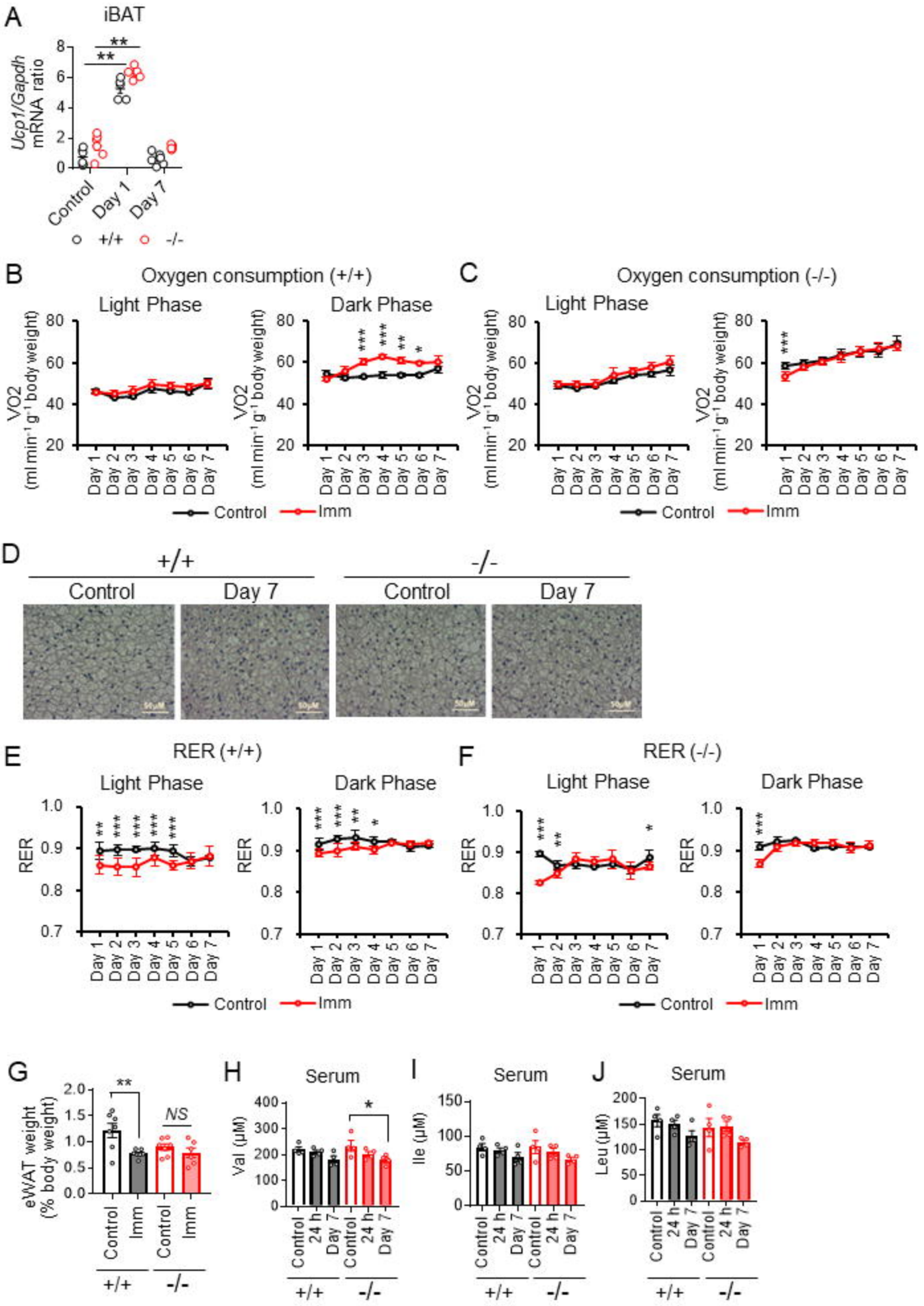

Figure 6_figure supplement 1

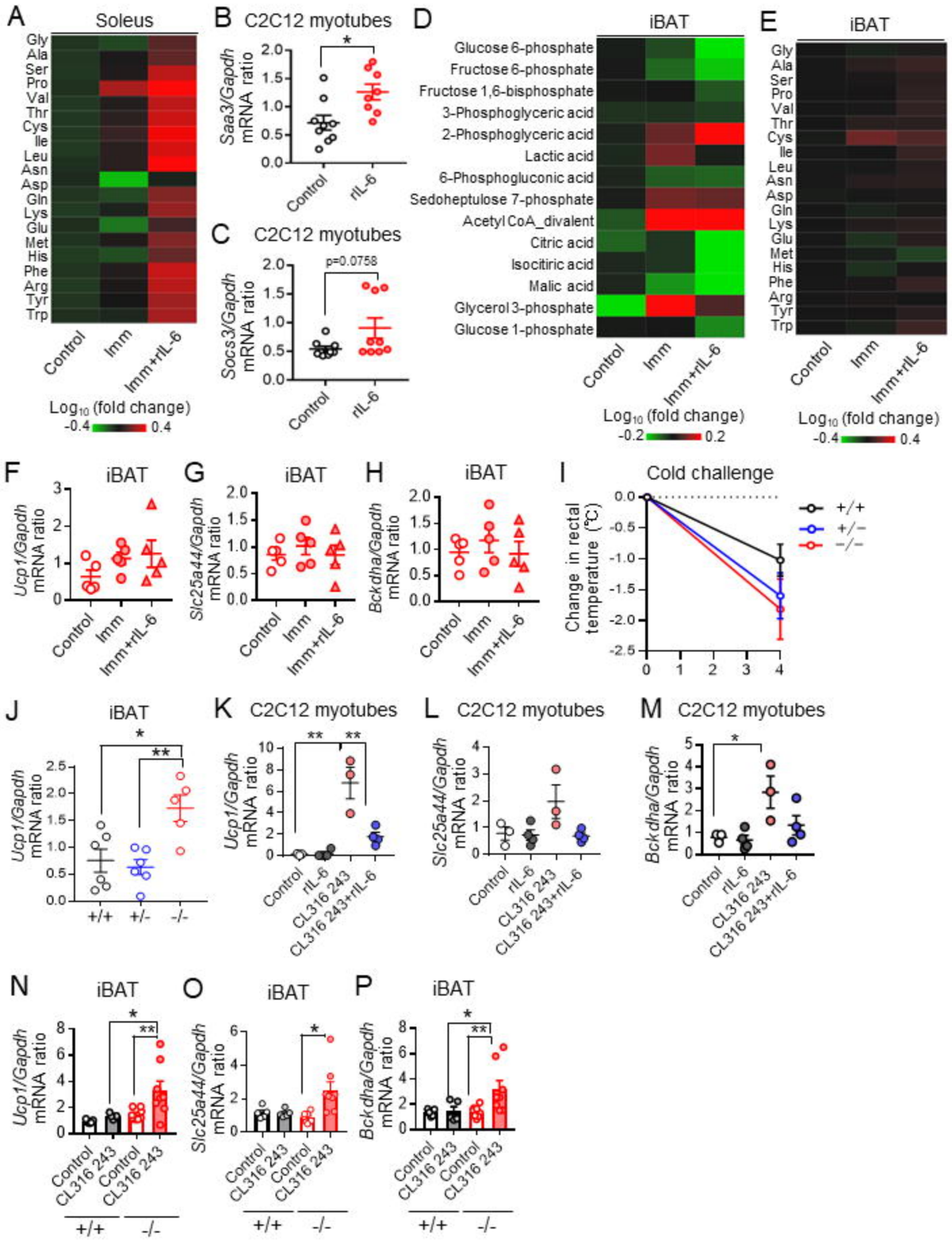

Figure 6_figure supplement 2

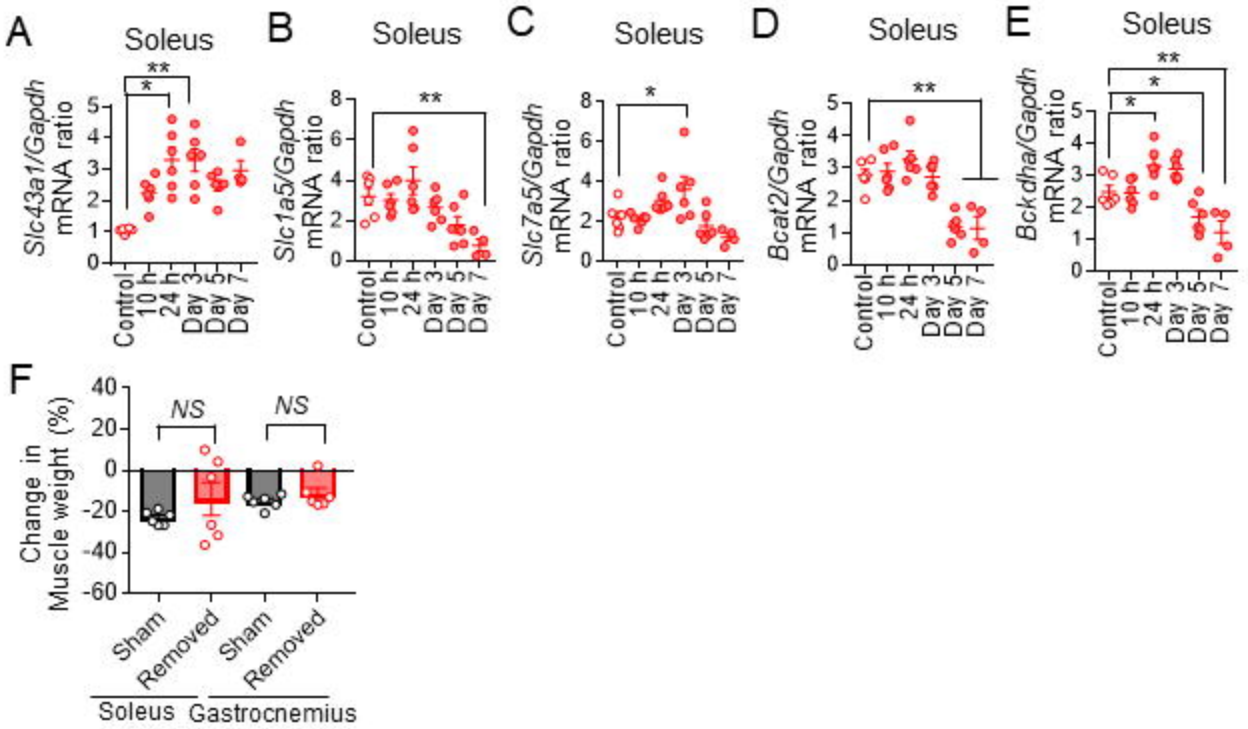

Figure 7_figure supplement 1

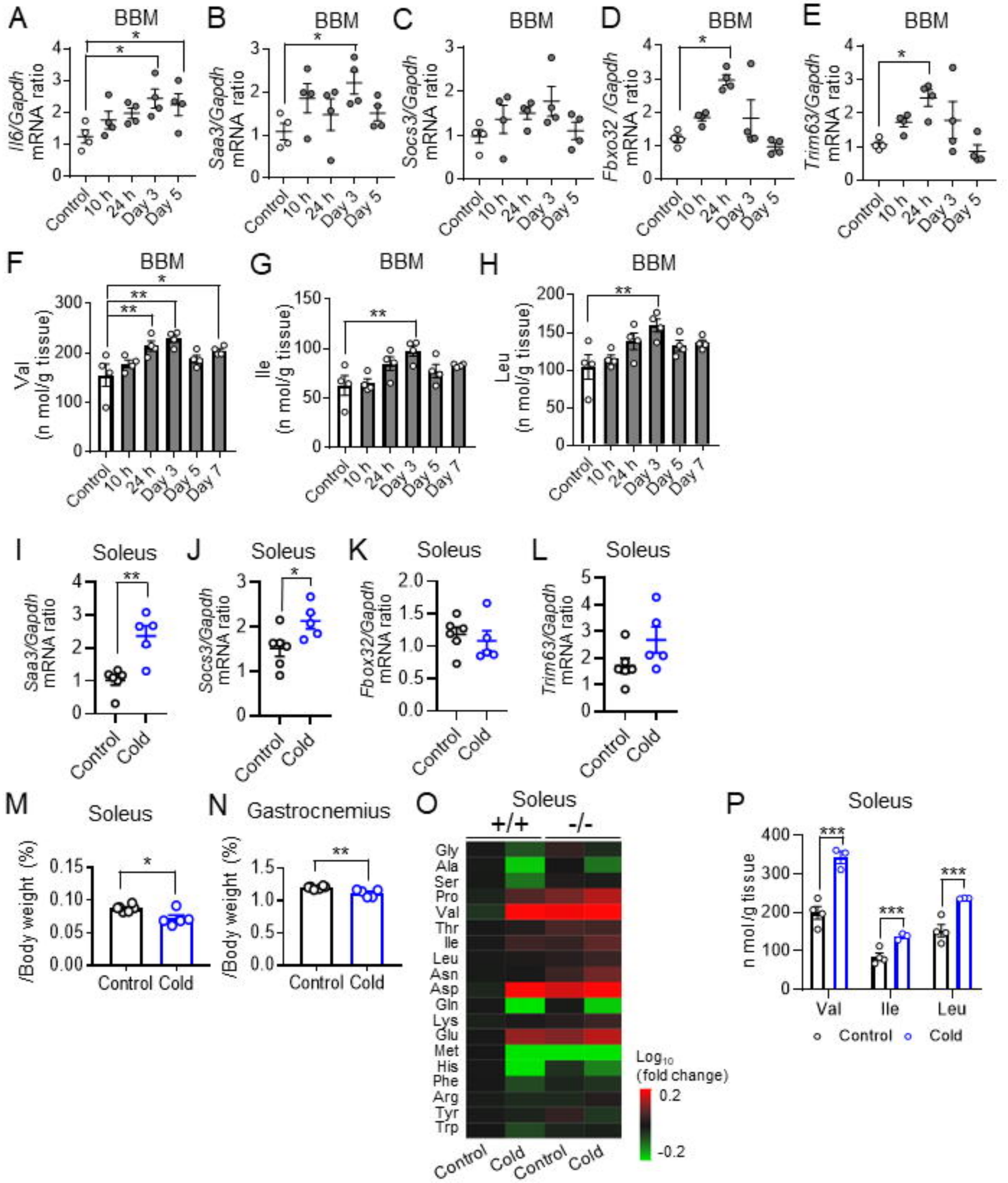
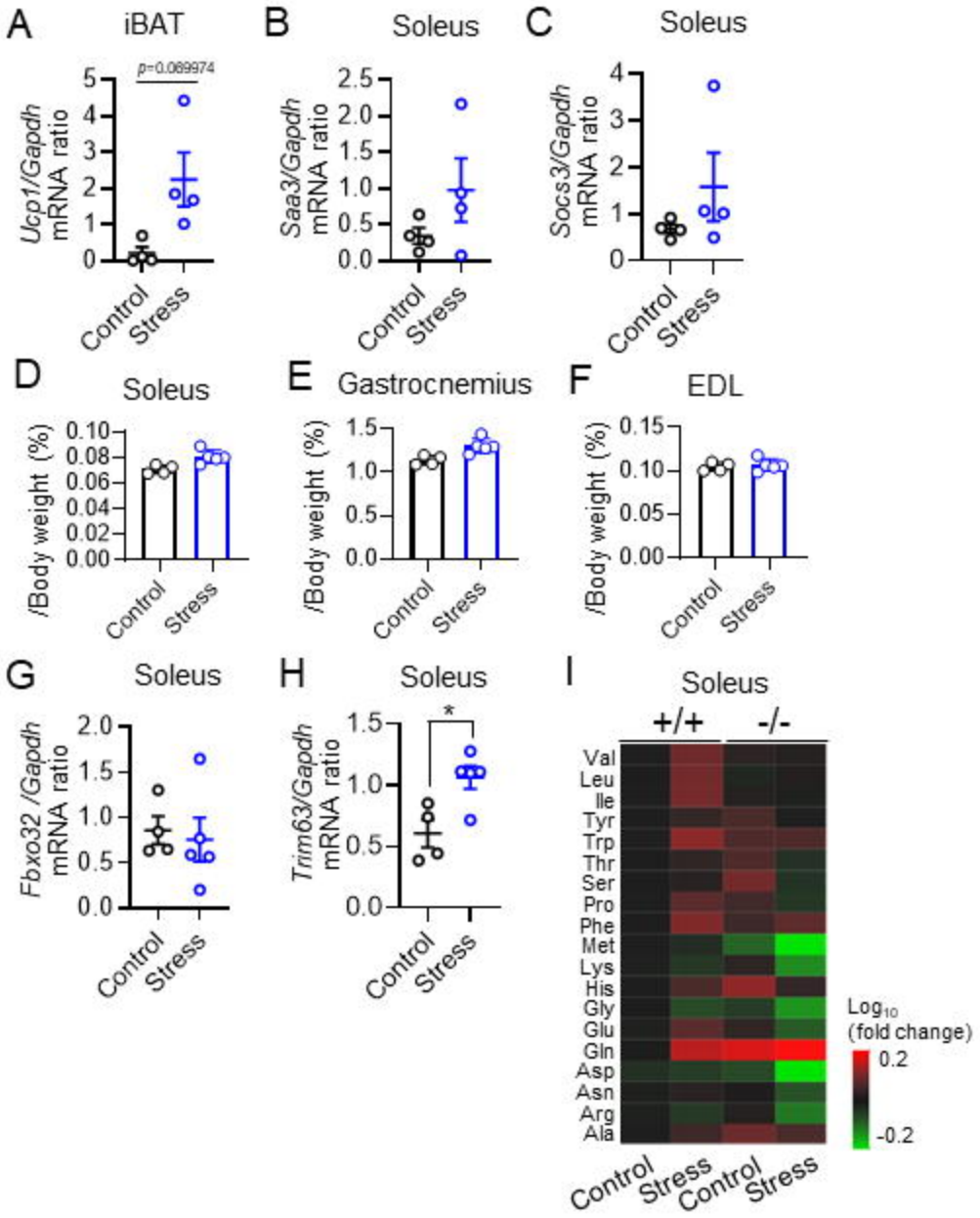
Figure 7_figure supplement 2